

## Part One

### Molecular/Local Spectroscopies



# 1

## Infrared Spectroscopy

*Frédéric Thibault-Starzyk and Françoise Maugé*

### 1.1

#### Introduction

Infrared (IR) light was discovered by Herschel in 1800 [1, 2] and the first commercial IR spectrometers appeared during World War II. IR spectroscopy has been used to study powdered heterogeneous catalysts since the 1960s, and *in situ* studies of working catalysts were first published in the 1970s [3]. IR spectroscopy underwent a complete renaissance when Fourier transform (FT) instruments became available in the 1980s, greatly improving the sensitivity of the technique and the quality of the spectra. Routine FTIR spectrometers appeared in chemistry laboratories around 1980. Their price has decreased steadily over time, and also that of the necessary hardware for mathematical treatment. Most heterogeneous catalysis laboratories now have an IR spectrometer, and it is now one of the basic techniques for the characterization of heterogeneous catalysts [4, 5]. Commercial cells are available for *in situ* IR studies during reactivity tests, leading to a steady increase in the number of publications in *in situ* IR spectroscopy. More than 15% of papers published in the field of heterogeneous catalysis present IR results. Our aim here is to give the beginner the necessary background and basic knowledge to start an IR study of their material. Experimental aspects will be presented, with the important points that should not be overlooked in order to obtain valid results. The complex spectra obtained by IR spectroscopy on the surface of a catalyst contain a true wealth of information. We have attempted to cover all of the main points, and give directions for further exploration.

### 1.2

#### Principles of IR Spectroscopy and Basic Knowledge for Its Use

##### 1.2.1

#### IR Light

The mid-IR region, in which we are interested here, covers the range of the electromagnetic spectrum from 25 to 2.5  $\mu\text{m}$ , that is, in wavenumber terms, from

400 to 4000  $\text{cm}^{-1}$ . The frequency of the radiation is denoted by  $\nu$ , and the wavelength is  $\lambda = c/\nu$ .

The unit used in IR spectroscopy is the wavenumber,  $\bar{\nu} = 1/\lambda = \nu/c$ . It is the number of periods (number of waves) observed per centimeter, hence the wavenumber unit is  $\text{cm}^{-1}$ .

The energy of the quanta associated to the radiation is proportional to  $\nu$  (and to  $\bar{\nu}$ ):  
 $E = h\nu$ .

### 1.2.2

#### Matter–Radiation Interaction

Depending on the frequency and on the type of interaction with matter, various spectroscopic techniques can be developed. Radiation with a given frequency  $\nu$  can change the energy of a system from the level  $E_i$  to the level  $E_f$  (and this radiation can thus be absorbed) only if that frequency is

$$\nu = \frac{E_f - E_i}{h}$$

Only the vibrations corresponding to a variation in the dipole moment in the molecule will lead to an absorption band in IR spectroscopy (the others will be active in Raman). In the mid-IR region, the radiation energy corresponds to changes in molecular vibration and rotation energies. The IR radiation will therefore be capable of changing the speed of rotations and vibrations in molecules each time it is tuned to the corresponding energies. The rotation energy is much lower than the vibration energy, and they will be observed in the lower region of the spectrum (lower  $\bar{\nu}$ ). With lighter atoms, and with greater bond strengths, faster vibrations are observed in the higher wavenumber region. IR bands at lower wavenumbers will be observed with heavier atoms and with weaker bonds. Heavy and large atoms and molecules will rotate more slowly and will lead to rotation levels with IR bands in the low  $\bar{\nu}$  region, towards the far-IR and microwave regions.

### 1.2.3

#### Spectrometry, Interferometry

Older spectrometers analyzed light with the aid of a monochromator. Wavelengths were analyzed in sequence, by dispersing light using a prism or a grid. Modern spectrometers are based on an interferometer. All wavenumbers are analyzed simultaneously and are digitally distinguished by Fourier analysis. The gain in energy is huge, since the whole of the light beam is collected.

In an interferometer (Figure 1.1), the light beam is divided into two on a beamsplitter before it reaches the sample. The two beams are recombined by two mirrors and sent to the sample, but one of the mirrors is mobile and can create a longer or shorter path on the way to the sample. The two beams will interfere depending on the path difference  $\delta$ . During the measurement, the moving mirror scans so that the intensity ( $V$ ) of the light collected on the detector depends on the

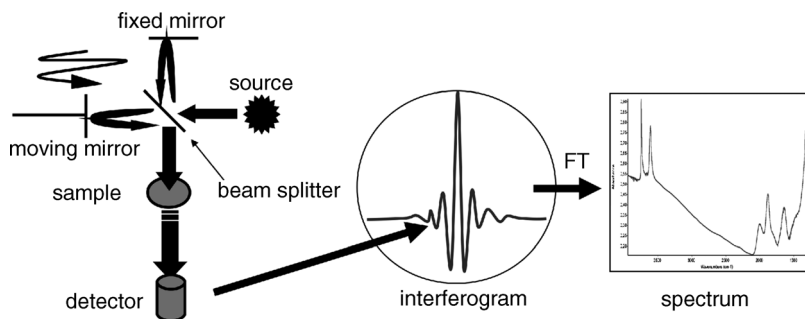


**Figure 1.1** Design of an interferometric spectrometer.

intensity of the light from the source ( $I$ ), on the frequency ( $\nu_0$ ) of the light, and on the position of the mirror (constructive or destructive interference depending on  $\delta$ ):

$$V(\delta) = I[1 + \cos(2\pi\nu_0\delta)]$$

The interferogram (intensity as a function of the path difference) is a sine function (more exactly, a cosine function) (Figure 1.2). The Fourier transform will lead back to the value of  $\nu_0$ :

$$I(\nu) = \int V(\delta) \cos(2\pi\nu\delta) d\delta$$

With polychromatic light, the interferogram will be the sum of several cosine functions with various periods: they all co-add in the middle ( $\delta = 0$ ), and add more and more destructively with increasing  $\delta$ , eventually summing to zero at infinite path difference (Figure 1.3). With increasing number of cosine functions, the results resemble more and more the typical interferogram observed on an interferometer for polychromatic light.

Fourier's theory states that any complex function can be analyzed as the sum of sine functions. The Fourier transform allows these functions to be re-found, and will yield the frequencies of the bands present in the interferogram. A continuous source is considered as the sum of an infinite number of bands. From the difference between

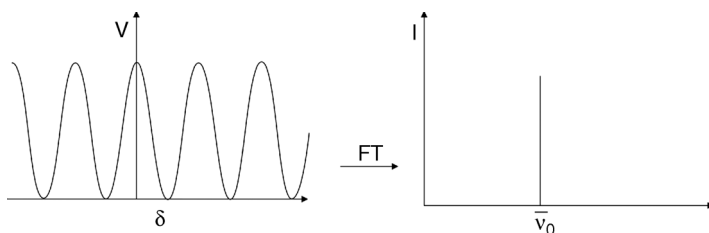


**Figure 1.2** Interferogram of a monochromatic light and its Fourier transform (only the positive part of the Fourier transform is shown).

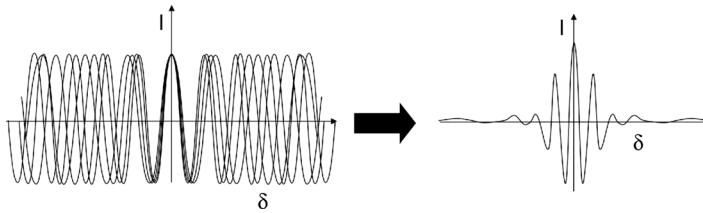


**Figure 1.3** Sum of cosine functions with various periods, forming the interferogram of a polychromatic light.

the spectrum of the instrument (so-called background spectrum) and the spectrum of the instrument plus sample, the spectrum of the sample can be obtained.

#### 1.2.4

#### Limitations of and Problems with the Fourier Transform

This method can only be applied rigorously when the integration is done between  $-\infty$  and  $+\infty$ , but the measurement is (usually) only done between the limits of the movement of the mirror with a path difference between  $-l$  and  $+l$ . The interferogram is thus actually the convolution product between the “infinite” interferogram and a rectangular function. The Fourier transform of a rectangular function is a sinc function (cardinal sine) (Figure 1.4).

Each spectral line will therefore be convoluted with this sinc function. It will be deformed, and shaped similarly to the sinc function. Each line, if assumed initially to be infinitely narrow, will be enlarged and will have side bands. These lobes can be removed by decreasing the relative contribution of the sides of the interferogram, by convoluting it with another function such as triangular, Happ–Genzel, and so on. This method is called apodization (removal of band feet). The main drawback is band broadening. The minimum width of the lines obtained is therefore linked to the integration limits  $-l$  and  $+l$  and to the path of the mirror. The larger the rectangular function (the greater the move of the mirror), the better is the spectral resolution.

To improve the graphical aspect of the spectrum, by a method very close to an interpolation, the size of the interferogram can be artificially increased by adding

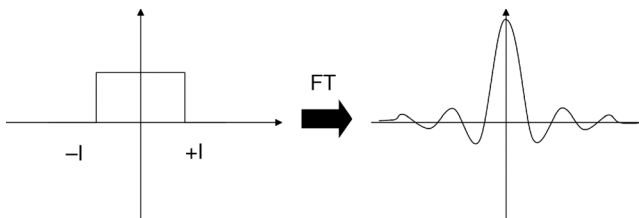


**Figure 1.4** Rectangular function (path difference between  $-l$  and  $+l$ ) and its Fourier transform, the sinc function.

zeros on its sides, where the values will anyway be very close to zero. This is called zero filling. A doubling of the size of the interferogram corresponds to a zero filling factor of 2, and so on. The spectrum is in this way smoothed in agreement with the interferogram. Despite the possible observation of new lobes on some lines, this computing trick does not improve the spectral resolution, in contrast to a greater path difference with the moving mirror. No new information is added to the interferogram, but better advantage is taken of it. On solids (and for adsorbed phases) the intrinsic width of the bands is large, and there is no need to work at a resolution better than  $2\text{ cm}^{-1}$ , but in order to obtain the best accuracy on the position of the band, one or two levels of zero filling are needed. By decreasing the “optical” resolution, the displacement of the moving mirror is limited, and so is the time needed for the complete scan. This is useful for improving time resolution for *in situ* or *operando* experiments.

### 1.3

#### Experimental Considerations

##### 1.3.1

#### Technical Aspects of the Fourier Transform

The IR signal is digitalized to obtain the numerical data for the Fourier transform. The analog to digital converter must be very precisely synchronized with the movement of the moving mirror, and the position of this mirror must be known continuously with great accuracy. A second light, perfectly monochromatic (an He–Ne laser at  $15\,798\text{ cm}^{-1}$ ), is used to form a secondary interferogram that will be used just for that purpose. This second interferogram is a sine function of the optical retardation (path difference). One point of the main interferogram will be collected each time the second interferogram is at its maximum (when the sine function is 1), that is, every  $0.3164\text{ }\mu\text{m}$  during the course of the mirror. The stability of the laser and of the electric zero for the instrument will therefore be of paramount importance for the reliability of the spectrometer. This will provide the interval for the sampling, and the next step will be to determine the origin of the interferogram: the point where the path difference with the moving mirror is zero (zero path difference, ZPD). This is usually taken as the maximum value for the IR interferogram.

The IR source is usually a globar (glowing bar): a rod of silicon carbide heated by an electric current, at temperatures between  $800\text{ K}$  ( $4500\text{--}300\text{ cm}^{-1}$ ) and  $1200\text{ K}$  ( $8000\text{--}50\text{ cm}^{-1}$ ).

Two main types of detectors are used, thermal (measuring heat on a target) and quantum detectors (counting photons) with different sensitivity, response speed, and spectral range. Thermal detectors are also called DTGS (deuterated triglycine sulfate), and quantum detectors MCT (mercury–cadmium–tellurium), type A or B, cooled with liquid nitrogen. Much more sensitive and faster, MCT detectors are also much more expensive. They are needed for *operando* studies, or for working in diffuse reflection mode. DTGS detectors quickly lose sensitivity with increasing ambient

temperature, but their response is more linear with increasing absorbance (at low signal).

The nature of the beamsplitter will influence the available spectral range of the spectrometer. It is KBr for the mid-infrared region, and extended KBr beamsplitters allow working from 400 to 7000 or 8000  $\text{cm}^{-1}$ , which is clearly a strong advantage for studying OH groups (these beamsplitters provide more energy between 3500 and 4000  $\text{cm}^{-1}$ ) or for harmonics and combination bands. For the near- or far-IR regions (not very commonly used in catalysis), specific beamsplitters are employed (quartz or  $\text{CaF}_2$ , and CsI or Mylar, respectively).

### 1.3.2

#### Practical Implementation

We present here some general experimental considerations for IR spectroscopy. The experimental setup for each type of experiment will be presented in the corresponding sections: *in situ* and static conditions in Section 1.4.2.1, and operando and flow conditions in Section 1.5.1.

##### 1.3.2.1 Transmission Experiments, Quantitative Aspects

Most often, IR experiments are performed in the transmission mode (Figure 1.5). The light passes through the sample, which is simply placed in the IR beam, between the source (incident intensity  $I_{0\nu}$ , at frequency  $\nu$ ) and the detector (measured intensity  $I_\nu$ ).  $I_{R\nu}$  is the intensity reflected by the sample; it does not reach the detector. For quantitative modeling, the sample is assumed to behave like a parallel-faced plate (thickness  $e$ ).

Kirchhoff's law is

$$T + \rho + A = 1$$

where  $T$  is the transmittance ( $I/I_0$ ),  $\rho$  is the reflectance ( $I_R/I_0$ ), and  $A$  is the absorption, energy absorbed by the sample (and diffused away from the detector). In transmission experiments, reflected and diffused energies are kept as low as possible, and are actually neglected. The measured value is  $T$ , which can be transformed in absorbance, or optical density:  $d = \log(1/T)$  (a decimal logarithm is used here, but

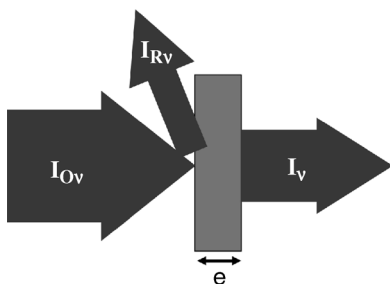


**Figure 1.5** The transmission experiment.

some spectroscopists, especially in Russia, use the natural logarithm, which can completely modify the values and the molar absorbance coefficients).

Light attenuation follows the Beer–Lambert law:

$$T = I/I_0 = \exp(-\kappa_\nu c\ell)$$

where  $\ell$  is the sample thickness,  $c$  is the concentration of absorbing species, and  $\kappa_\nu$  is the molar absorption coefficient (in  $\text{mol}^{-1} \text{dm}^3 \text{m}^{-1}$ ) at frequency  $\nu$ . This law can also be written in terms of the optical density:

$$d = \varepsilon_\nu c\ell$$

where  $\varepsilon_\nu$  is then the molar absorption coefficient (also in  $\text{mol}^{-1} \text{dm}^3 \text{cm}^{-1}$ ) and  $\varepsilon = \kappa/2.3$ . It is noteworthy that in powders, the particle size influences  $\varepsilon$ , which slightly increases with decreasing particle size. In the commonly used pellets,  $\varepsilon$  is not directly accessible. The amount of species interacting with the light beam is  $c\ell$ , and the following expression is used:

$$c\ell = n/S$$

where  $n$  is the number of adsorbing species in the pellet and  $S$  is the area of the pellet. It follows that

$$d = \varepsilon_\nu \left( \frac{n \times 10^{-3}}{S} \right)$$

with  $n$  in  $\mu\text{mol}$ . Depending on authors, and in order to simplify the equations, the units used for  $\varepsilon$  are commonly  $\text{mol}^{-1} \text{dm}^3 \text{cm}^{-1}$ , or  $\text{mol}^{-1} \text{cm}^2$  (1000 times difference). The maximum absorbance or integrated area can be used for measuring a band. The latter is much more sensitive to baseline perturbations, but much less to differences in temperature or resolution. The integrated area is expressed in  $\text{cm}^{-1}$ , and the molar absorption coefficient will then be expressed in  $\text{mol}^{-1} \text{cm}$ , or more commonly in  $\mu\text{mol}^{-1} \text{cm}$ . On solids, calibration curves are necessary, and the Beer–Lambert law is not always valid (especially with hydrogen bonds [6]).

### 1.3.2.2 Diffuse Reflection

Diffuse reflection is another technique for measuring the IR spectrum. It became popular with the increased sensitivity of detectors and of FT spectrometers, and with available commercial cells. The light is no longer observed through a wafer, but reflected in all directions by the powder. The tedious and difficult task of making the wafer is avoided, and the powder is simply placed in a cup.

The light that hits the powder can be reflected as on the surface of a mirror, and this is specular reflection. Light can also penetrate the sample and be partly absorbed or transmitted further. The penetrating light can also be partially absorbed, reflected, and refracted inside the sample, and diffused back towards the surface of the sample; this is diffuse reflection (Figure 1.6).

If the sample is thick enough (a few millimeters), the intensity passing through the sample will be zero. If the specular reflection is weak enough (matt surface, fine

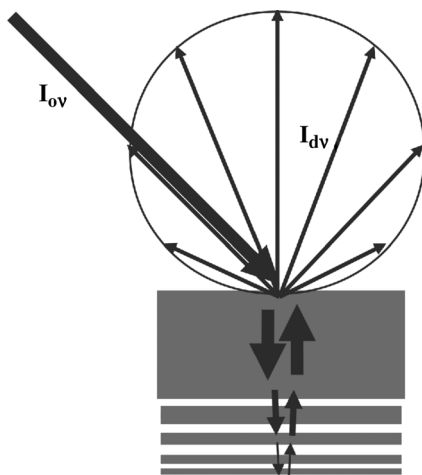


**Figure 1.6** The diffuse reflection experiment.

powder), then the intensity of diffused light  $I_d$  will provide information about absorbed light in the sample. For a sample dispersed in a nonabsorbing matrix (such as KBr), the resulting spectrum is very similar to a spectrum recorded in transmission mode. However, the quantitative laws are not the same. The Kubelka–Munk function can be used to convert data so that band intensities are (to a first approximation) proportional to the amount of species observed. Optical density (absorbance units) can still be used for very weak bands, since the Kubelka–Munk function tends to be proportional to concentration at low absorbed intensity. It is, however, a misuse (absorbance is defined together with transmittance; it should be defined here with reflectance) and this approximation ceases to be correct as soon as the intensity increases.

The signal obtained depends on the light diffusion coefficient in the material. This coefficient is strongly linked to particle size, and depends directly on the ratio between particle size and wavelength. When the particle size is of the same order of magnitude as the wavelength, band intensities are linearly proportional to the wavelength. With smaller particles, bands are narrower, but their intensity is even more dependent on the wavelength. With larger particles, the intensity is more constant (but bands are broader). However, using the same molar absorption coefficient as in transmission is not possible.

Band intensities in diffuse reflection are also very much influenced by the temperature, which influences the diffusion coefficient in solids. Specular reflection can also be (relatively) important in spectral regions close to strong absorptions, and “false transparency” regions can appear in the spectrum (especially around structure vibrations in oxides). Checking the transmission spectrum is therefore an important aid before spending much time on the interpretation of the diffuse reflection spectra of solids.

## 1.4 Use of IR Spectroscopy to Characterize Solids

### 1.4.1 IR Spectrum and Structure of a Solid

The easiest way to measure the IR spectrum of a solid is to place the powder as a suspension in a neutral oil (Nujol) or, more generally, to disperse it (0.5–1%) in potassium bromide (KBr). The resulting powder is pressed ( $5\text{--}8\text{ ton cm}^{-2}$ ,  $5\text{--}8 \times 10^8\text{ Pa}$ ) to form a pellet placed directly in the IR beam. Such a method cannot be used for characterizing the surface properties of catalysts (e.g., with probe molecule adsorption studies), but can provide interesting information about the structure of the materials.

#### 1.4.1.1 The Example of Zeolites

The KBr matrix method is used as a very general approach for the initial characterization of zeolites. The main bands observed are due to structure vibrations between  $400$  and  $1300\text{ cm}^{-1}$  (Figure 1.7). These bands have been assigned to  $\nu(\text{T-O})$  vibrations:

- symmetrical:  $700\text{--}850\text{ cm}^{-1}$
- asymmetric:  $1000\text{--}1200\text{ cm}^{-1}$

Some of these were assigned to vibrations internal or external to the  $\text{TO}_4$  tetrahedra. Modeling of framework vibrations in zeolites showed that these bands could not be assigned to the vibration of any particular interatomic bond, but rather that they are all produced by the vibrations of the network as a whole.

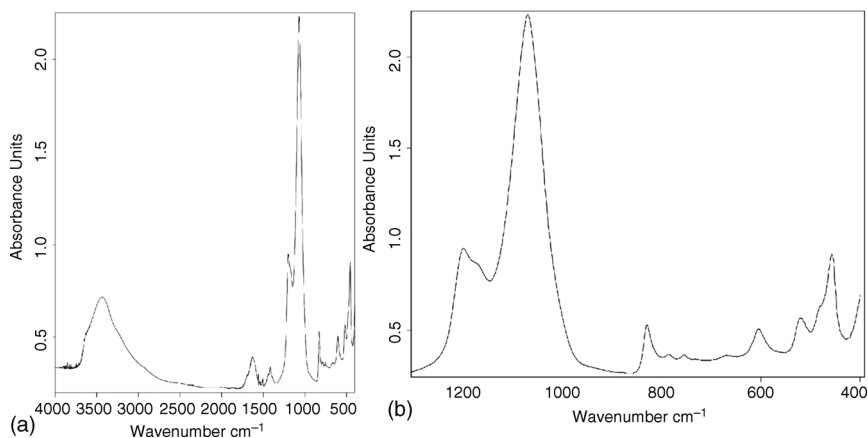


**Figure 1.7** (a) Spectrum of a steamed Y zeolite, as KBr matrix pellet. (b) Zoom on the range of the structure vibrations.

The intensity of some of these structure vibration bands changes linearly with the amount of aluminum in the framework, and they are therefore assumed to be mostly due to Al–O vibrations. They can sometimes be used to measure the Al content [number of framework Al atoms per unit cell  $N_{\text{Al(F)}}$ ]. Empirical relationships have been established between their frequency and the framework Si/Al ratio, as determined by other techniques such as NMR spectroscopy. The faujasite (FAU) structure is probably the one that has attracted the most attention in this area, especially in the pioneering work of Flanigen [7] and Lunsford [8]. For the bands at  $1050$  ( $\nu_1$ ) and  $810$   $\text{cm}^{-1}$  ( $\nu_2$ ), the following relations were determined:

$$N_{\text{Al(F)}} = 0.766(1066.7 - \nu_1)$$

$$N_{\text{Al(F)}} = 1.007(832.8 - \nu_2)$$

The frequency of these bands decrease with decreasing Si/Al ratio, but they are also influenced by any extra-framework phase present, and a vibration more specific to hexagonal prisms at  $600$   $\text{cm}^{-1}$  (and thus to the framework itself) is sometimes preferred. Chevreau and co-workers [9] showed that the frequency of this  $\nu_3$  band is linked to the aluminum concentration, and its intensity to the crystallinity of the sample (Figure 1.8):

$$N_{\text{Al(F)}} = -1.401\nu_3 + 856$$

It should be noted that cation exchange also influences the frequency of structure vibration bands in zeolites. Other structures are also well known: beta-zeolite [10] and mordenite [11]. In mordenite, the amount of Al per unit cell ( $\text{Al}_{\text{s/UC}}$ ) has been linked to the frequency of a  $\nu(\text{Al-O})$  vibration band at about  $650$   $\text{cm}^{-1}$ :

$$\nu(\text{Al-O}) = 654 - 4.6\text{Al}_{\text{s/UC}} \text{ in the absence of sodium}$$

$$\nu(\text{Al-O}) = 651 - 3.8\text{Al}_{\text{s/UC}} \text{ when sodium is present in the zeolite.}$$

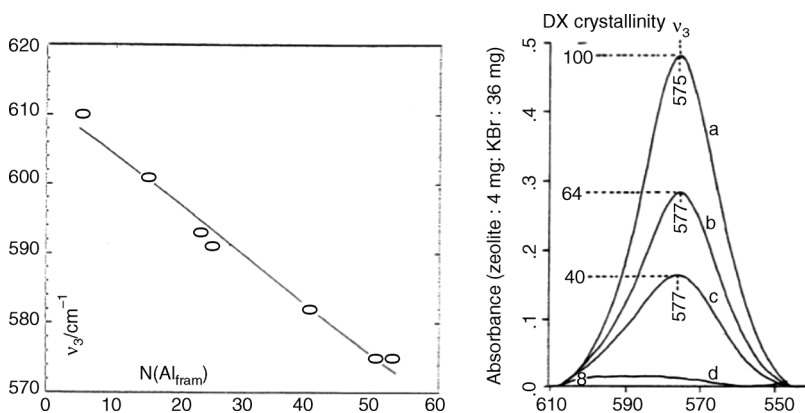


**Figure 1.8** Monitoring framework aluminum content and crystallinity using structure vibration bands [9].

#### 1.4.1.2 Substitution of Metals in the Structure of Zeolites

IR spectroscopy has been used for studying atom substitution in the framework of zeolites by looking at framework vibrations. In substitution by boron, for example, new bands can be detected at 1380, 920, 700 and 620  $\text{cm}^{-1}$  [ $\nu(\text{B-O})$  and  $\nu(\text{B-O-Si})$  vibration bands]. New Brønsted acid sites were also detected on introducing heteroelements in AlPOs, and a new  $\nu(\text{OH})$  band appearing in the 3500–4000  $\text{cm}^{-1}$  region can be another indication for the introduction of heteroelements.

#### 1.4.2

##### Activation: Cleaning the Sample to Observe Surface Sites

The surface properties of solid powders (acid sites or adsorption of reactants on catalysts, for example) can only be studied on the pure sample after removal of unwanted surface species (physisorbed species, water, etc.) by the so-called activation treatment. Valuable information on surface sites can be obtained from analysis of the OH groups (Section 1.4.3), from identification of residual impurities (Section 1.4.2.2.2), or by using adsorbed probe molecules (Section 1.4.4).

##### 1.4.2.1 Experimental Aspects

Most characterization work on surface properties is performed in the transmission mode. This should only be done with a self-supporting wafer of the pure solid, that is, without any KBr matrix that would contaminate the surface and introduce external ions. This wafer must be very thin (generally 10–20 mg for 2  $\text{cm}^2$ ) so that it remains IR transparent, and must only be pressed very gently ( $<500 \text{ kg cm}^{-2}$ ,  $5 \times 10^7 \text{ Pa}$ ) so that neither gas diffusion nor the structure of the solid are perturbed. This point must be strongly emphasized, since it is much easier to make a wafer by using higher pressure, but the quality of the results can be greatly affected, by damaging delicate crystal structures or by hindering gas diffusion and adsorption of probe molecules.

When the wafer is not thin enough, the energy collected by the detector will be too low: the spectrum will be noisy and (worse) the detector will not operate within its linearity range, leading to non-quantitative results. In order to avoid losing a linear response, the spectrum baseline must be low enough that bands do not reach intensities higher than 2 (or at very worst 3) in the range where no structure bands are present. This is especially true for liquid nitrogen-cooled MCT detectors, which are much more sensitive than the less expensive DTGS detectors, but for which this important drawback must be kept in mind.

Conversely, care must be taken to have very strong absorption of light by structure bands. If the optical density is not at least 4 (often 6) for the intense structure vibrations bands (typically below 1200  $\text{cm}^{-1}$ ), then energy reaches the detector where it should not. The wafer might be damaged (fractured) or wrongly aligned in the IR beam. Here again, no good quantitative results can be obtained.

**1.4.2.1.1 Infrared Cell for *In Situ* Studies** The wafer is placed in an IR cell allowing heating of the sample under vacuum and also adsorption of controlled doses (or a

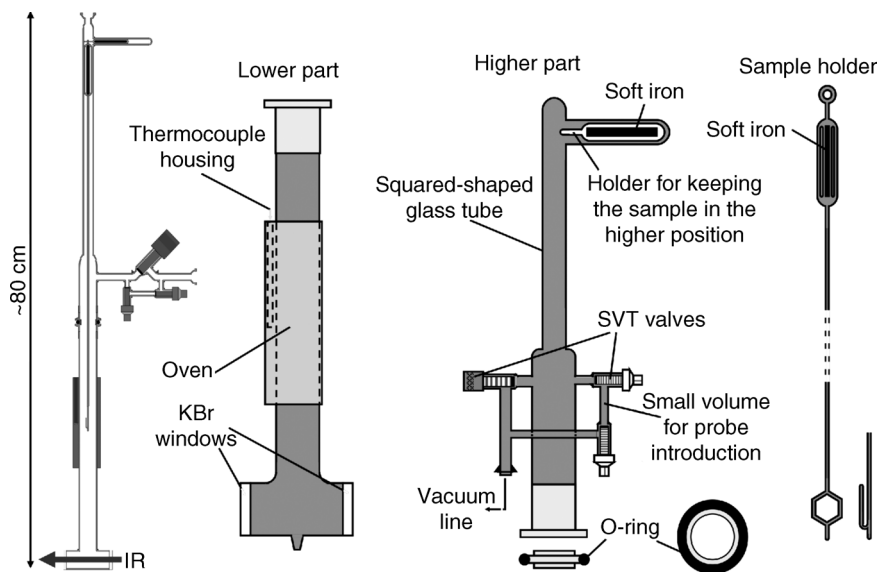


**Figure 1.9** IR cell for transmission studies of solid catalysts under a controlled atmosphere (*in situ* studies). The sample holder can be moved from the lower (IR beam) to the higher position (oven) without opening or moving the cell by using magnets as handles. (Drawing by P. Bazin).

flow) of gas (Figure 1.9). Heating is commonly applied outside the IR beam, and the sample holder can move between the heating position and the position for recording the IR spectrum in the beam. Some studies must be performed at low temperatures and this is done by cooling the bottom of the cell with liquid nitrogen (or another cooling agent).

Depending on the measurement, various experimental conditions can be needed, for example, heating to 750–950 K for activation, cooling to 100 K for some probe molecule adsorption, or heating under a gas flow and under high pressure for catalyst activation under the reaction conditions. Many different cells have been designed by various laboratories working in the field in order to obtain these conditions. Special cells were designed for studying the surface *in situ* in a dynamic mode, so that the catalyst can be under working conditions (*operando*). These are presented later (Section 1.5.1).

#### 1.4.2.2 Activation – Cleaning the Sample to Observe Surface Sites

Much useful information on a catalyst can be obtained during and after the activation process concerning the decomposition of organic precursors and formation of active sites.

**1.4.2.2.1 The Example of Zeolites** During activation of a zeolite, adsorbed water and any organic molecule such as the synthesis template are removed. The decrease in the amount of water can be monitored by the decrease in the intensities of the bands of

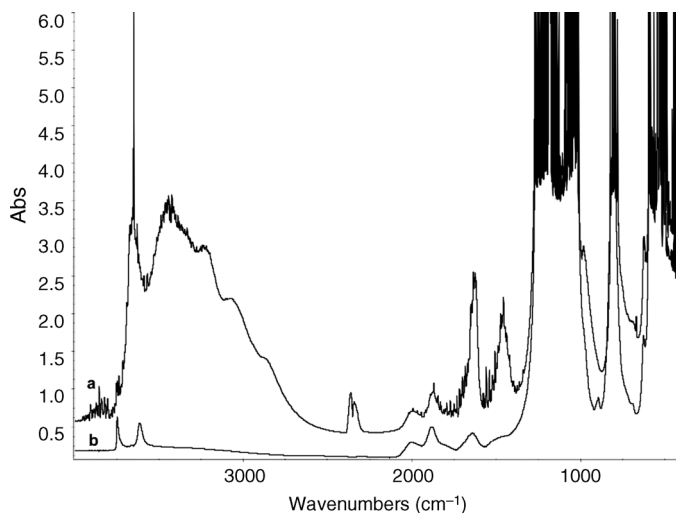


**Figure 1.10** Spectrum of an MFI-type zeolite, (a) before ( $\text{NH}_4\text{-MFI}$ ) and (b) after ( $\text{H-MFI}$ ) activation treatment. The intense structure bands are visible below  $1100\text{ cm}^{-1}$ , in addition to bands for water and ammonium before activation.

molecular water: the  $\nu(\text{OH})$  and the  $\delta(\text{OH})$  vibration bands (a very broad band around  $3500\text{ cm}^{-1}$  and a broad band at  $\sim 1630\text{ cm}^{-1}$  respectively) (Figure 1.10). For a zeolite in the  $\text{NH}_4^+$  form, the leaving ammonium group is visible as a band around  $1460\text{ cm}^{-1}$  and controlling the activation is easy.

Some very sensitive zeolites, such as mordenite and aluminum-rich zeolites can easily be damaged during activation, and a self-steaming process can take place when the thermal treatment is too fast, thus leading to an extra-framework phase in the solid. This can be checked after the activation by verifying the absence of any vibration bands for  $\text{AlOH}$  groups [ $\nu(\text{OH})$  bands around  $3660\text{ cm}^{-1}$ ] and by measuring the number of Lewis sites by pyridine adsorption at the end of the experiment (a defect-free zeolite should contain no Lewis sites) (Figure 1.11).

If the activation is aimed at removing the templating agent in a zeolite, the corresponding IR bands must first be identified, and their progressive disappearance can be directly monitored *in situ* during the calcination treatment (Figure 1.12). These organic species cannot be removed by heating the solid under vacuum, but rather under air or a few torr of ozone.

**1.4.2.2.2 Residual Impurities** After metal oxide activation, even at high temperatures ( $>773\text{ K}$ ), some bands below  $1600\text{ cm}^{-1}$  could remain. They characterize the presence of remaining impurities, which are related to the history of the material (including the nature of the precursors or the solvent used for metal oxide preparation). The identification of the nature, structure, and amount of residual impurities such as carbonate, nitrate, and sulfate species, is important since they can modify the properties of the pure metal oxides, by blocking the accessibility of reactant to surface

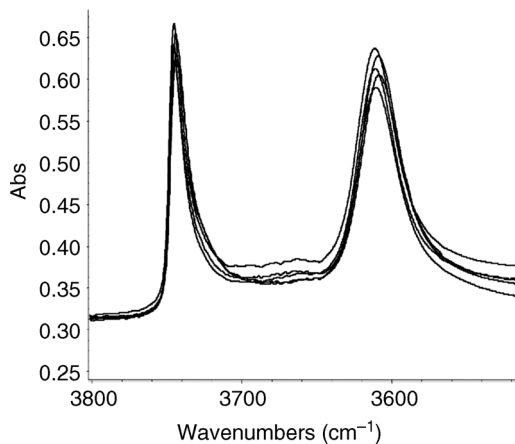


**Figure 1.11**  $\nu(\text{OH})$  bands in MFI-type zeolites after various calcination procedures. Weak bands are visible around  $3660\text{ cm}^{-1}$  showing the presence of an extra-framework aluminic phase in some of the samples.

sites, or by generating Brønsted and Lewis acidity (basicity) at the expense of the intrinsic basicity (acidity).

**Carbonates** The contact of the  $\text{CO}_2$  present in air with metal oxide basic sites, such as oxygen or OH anions, leads to the formation of carbonate or hydrogencarbonate

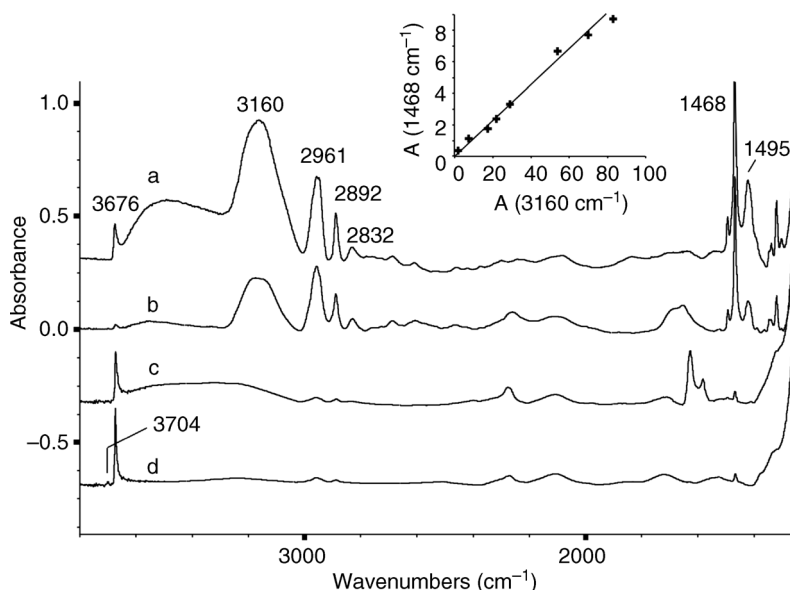


**Figure 1.12** *In situ* calcination (from a to d) of cloverite under ozone in the IR cell [12]. The bands at  $1468$  and  $3160\text{ cm}^{-1}$  are assigned to the template, and their progressive disappearance shows the corresponding increase in free OH groups on the surface (after evacuation, spectrum d).

groups, respectively. The free carbonate ion ( $D_{3h}$  symmetry) presents one asymmetric  $\nu(\text{CO})$  vibration at  $1415\text{ cm}^{-1}$ . In the adsorbed state, its symmetry is lowered and two  $\nu_3(\text{CO})$  bands appear as a result of the splitting of the degenerate asymmetric  $\nu(\text{CO})$  vibration. The  $\Delta\nu_3$  splitting is thought to characterize the structure of the species formed. Hence different structures of carbonate species can be identified as unidentate, bidentate, and bridging carbonates with a  $\Delta\nu_3$  of about 100, 300, and  $400\text{ cm}^{-1}$ , respectively. Thermal stability can also be a way to differentiate these species since unidentate are less stable than bidentate carbonates. Carbonate species with a strong resistance to thermal decomposition and a fairly low  $\Delta\nu_3$  splitting can correspond to a polydentate structure, that is, a bulk-like or subsurface species.

**Nitrates** Similarly to carbonates, the free nitrate anion has  $D_{3h}$  symmetry. Two  $\nu_3(\text{NO})$  bands appear with adsorbed nitrates (instead of only one at  $1380\text{ cm}^{-1}$  for the free anion) and the  $\nu(\text{NO})$  at  $\sim 1050\text{ cm}^{-1}$  becomes IR active (instead of being only Raman active). Similarly to carbonate ions, the splitting of the  $\nu_3(\text{NO})$  vibration and its thermal stability are greater for bidentate than for monodentate species. The similarity between  $\text{NO}_3^-$  and  $\text{CO}_3^{2-}$  spectra can lead to difficult band assignments when both species are present.

**Sulfates** Surface sulfate species on activated oxides are characterized by a band at  $\sim 1340\text{ cm}^{-1}$  together with several bands below  $1260\text{ cm}^{-1}$ . They are specific to the single S = O group with the sulfur atom anchored to the oxide surface through three S–O–M linkages. Stable bulk surface species can also be formed on oxide presenting strong basic properties.

Note that other contaminants, such as chloride or sodium ions, could also be present but they do not lead to any characteristic IR band. However, it should be kept in mind that their presence could strongly modify oxide surface properties.

### 1.4.3

#### The Spectrum of OH Groups

The surfaces of metal oxides are preferentially terminated by hydroxyl groups, leading to important patterns in the mid-IR spectrum. The IR bands for OH groups can be  $\nu(\text{OH})$ ,  $\delta(\text{OH})$ , or  $\gamma(\text{OH})$ . Elongation vibrations in OH groups are denoted  $\nu(\text{OH})$ . They produce absorption bands in the IR spectrum between  $3500$  and  $3800\text{ cm}^{-1}$ . The  $\delta(\text{OH})$  vibration is a deformation of the OH bond parallel to the plane of the two bonds on the oxygen atom (in-plane deformation). It leads to a band in the middle part of the mid-IR spectrum, between  $1200$  and  $2000\text{ cm}^{-1}$ . The  $\gamma(\text{OH})$  vibration is a deformation of the OH group out of the plane of the bonds on the O atom, leading to an IR band in the low-frequency region, usually below  $1500\text{ cm}^{-1}$ .

The free hydroxyl groups gives a unique fingerprint of the acid sites (Brønsted acidity in oxides is brought about by the presence of OH groups), but also give indications on the structure of the subsurface oxide.

Theoretical studies helped in understanding the various parameters influencing the frequency of the  $\nu(\text{OH})$  band: the coordination number of the oxygen atom, the

coordination number of the neighboring cation (M), the location on defective crystal configurations (edge, corner or kink), the presence of cationic vacancies in the direct vicinity of the OH group, the electronegativity of the cation, and the oxidation state of the cation. DFT calculations indicate the presence of H-bonded OH groups even after oxide activation. Such bonds, of course, also strongly influence the frequency of the  $\nu(\text{OH})$  vibration.

Experiments and *ab initio* calculations both show that the  $\nu(\text{OH})$  frequency decreases when the number of associated cations M increases. This is in good agreement with the empirical basis assuming that cations have an electron-withdrawing effect on the electronic density of the OH group, then increasing the polarization of the OH bond. The frequency of these bands can be used as a first indication of the strength of the corresponding Brønsted sites: the stronger the acidity of the OH group, the lower is the electronic density between the oxygen and the hydrogen atoms (the bond strength decreases) and the lower the  $\nu(\text{OH})$  band frequency. This is not, however, a direct measurement of acidity, and this rule is often not valid. The  $\nu(\text{OH})$  frequency has a similar value,  $3745 \pm 3 \text{ cm}^{-1}$ , for a basic oxide such as MgO, for a weakly acidic amorphous silica, and for a strongly Brønsted acid such as amorphous silica–alumina [13]. The frequency of the  $\nu(\text{OH})$  band is strongly influenced by the local environment of the site, by the presence of neighboring OH groups or oxygen atoms (linked to the size of the pores and to the presence of the extra-framework phase in zeolites). The frequency of the  $\nu(\text{OH})$  vibration bands therefore cannot be used for the comparison of acid strengths in different solids, and not even for various sites located differently on the same solid.

#### 1.4.3.1 OH Groups on Alumina

On alumina, at least five  $\nu(\text{OH})$  bands can be detected (at about 3790, 3770, 3755, 3730, and 3680  $\text{cm}^{-1}$ ). In the 1970s, several empirical models were proposed to account for these various OH groups. Considering the coordination number of bulk alumina oxygen atoms (4), only three types of surface OH groups are expected (referred to as type I, II, and III) [14]. Taking into account the different coordination numbers of aluminum cations (IV and VI), and the structure of the preferentially exposed planes of  $\gamma$ -alumina, Knözinger and Ratnasamy identified five different OH groups [15]. In more recent work using DFT calculations, Digne *et al.* proposed some differences in the assignments of the  $\nu(\text{OH})$  bands, but the general trends are similar [16].

#### 1.4.3.2 OH Groups in Zeolites

Several different types of OH groups can be distinguished in zeolites. The two main types of sites are easily observed in MFI-type zeolites (Figures 1.10 and 1.11):

- 3745  $\text{cm}^{-1}$ : vibration of isolated silanol groups, similar to those observed in silica, very weakly acidic
- 3610  $\text{cm}^{-1}$ : bridged hydroxyl groups ( $\text{SiOHAl}$ ), Brønsted acid sites.

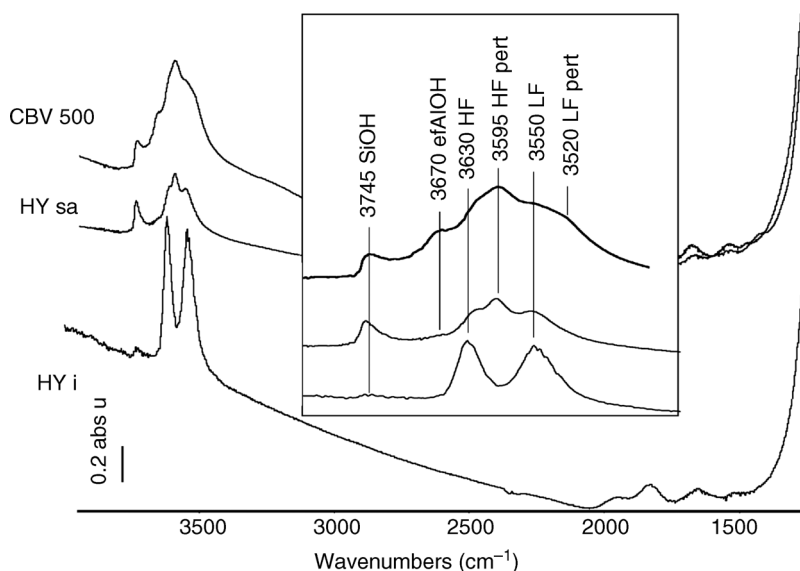


**Figure 1.13** Spectra of activated HY zeolites: modified by isomorphic substitution (HYi), steamed and acid washed (HYsa), and industrially steam treated (CBV500). The inset shows a detail of the  $\nu(\text{OH})$ , with silanols at  $3740\text{ cm}^{-1}$ , OH groups in large cavities (HF at  $3615\text{ cm}^{-1}$ ) and in hexagonal prisms and

sodalite cavities (LF at  $3555\text{ cm}^{-1}$ ). OH groups perturbed by extra-framework phase  $\text{HF}_{\text{pert}}$  and  $\text{BF}_{\text{pert}}$  are visible on steamed samples. The OH corresponding to the  $\text{HF}_{\text{pert}}$  is sometimes described as superacidic. The band at  $3660\text{ cm}^{-1}$  comes from the  $\nu(\text{AlO-H})$  vibration in the extra-framework aluminic phase.

In the H-MFI zeolite, these bridged OH groups only lead to one  $\nu(\text{OH})$  vibration band, but in more complex structures such as mordenites or faujasites, the number of different  $\nu(\text{OH})$  bands increases. In the example of Y zeolite (Figure 1.13), we also observe:

- $3630\text{ cm}^{-1}$ : high-frequency (HF) band for OH in the supercages
- $3550\text{ cm}^{-1}$ : low-frequency (LF) band for OH groups in the sodalite units or hexagonal prisms of the structure.

When an extra-framework phase is also present in the sample, it will perturb the OH groups and produce additional bands:

- $3600\text{ cm}^{-1}$ : perturbed HF band bearing the strongest acidity (so-called enhanced acidity)
- $3520\text{ cm}^{-1}$ : perturbed LF band, probably also enhanced acidity, but out of reach for most molecules, and therefore without any direct role in acidity or catalysis.

Other nonacidic OH groups are also visible with lower intensity:

- $3660\text{--}3680\text{ cm}^{-1}$ : aluminic OH (extra-framework phase)
- $3775\text{--}3785\text{ cm}^{-1}$ : aluminic OH groups, often described as basic.

$\nu(\text{OH})$  bands are slightly shifted to lower wavenumbers with increasing temperature, and can be observed 15–20  $\text{cm}^{-1}$  lower at 450 °C than at ambient temperature. Upon heating, these bands also broaden. Conversely, on cooling (e.g., with liquid nitrogen for some adsorption studies), the  $\nu(\text{OH})$  bands become narrower and shift to higher wavenumbers.

$\nu(\text{OH})$  bands with very similar frequencies can correspond to Brønsted sites with very different acid strengths, and they can only be distinguished by the use of probe molecules.

#### 1.4.4

#### Characterization of Acidity with Probe Molecules

Acidity is in many cases the key point for catalytic activity. IR spectroscopy has long been used for the characterization of acidity since Brønsted acid sites are directly visible in the IR spectrum, and OH groups lead to very typical vibration bands. Lewis sites are most often not directly detected, and probe molecules must be employed.

IR spectroscopy is adapted to follow probe molecule adsorption on the catalyst surface, and thus to obtain information on the nature, strength, local arrangement, and amount of surface sites: acidic, basic, metal, or sulfide sites. On the choice of the probe molecule depends the type of information investigated [17].

A lot of information can be obtained by studying molecular interactions between a basic probe molecule and the surface of an acidic solid. Modifications in the spectrum of the probe molecule will indicate the type, strength, and density of sites on the surface. When an H-bond appears, its strength can be measured by IR spectroscopy, and corresponds to the acid strength of the site. Band intensities indicate the number of sites. The type of information obtained will be selected by carefully choosing the probe molecule for the study. Some probe molecules can even be used during the reaction for spectroscopic studies of the catalyst under working conditions (so-called *operando* studies, see the definition in Section 1.5). The ideal properties of IR probe molecules depending on the type of catalyst under study were given about 15 years ago by Lercher *et al.* [18] and Knoezinger *et al.* [19]. The basic strength, the size of the molecule, and its spectral response to a perturbation (band intensities and sensitivity of the frequency to the perturbation) are all important points. The molecule must be stable on the surface, and not be hydrolyzed or oxidized. It needs to be easily adsorbed on the solid (only vapors are introduced in the cell containing the solid sample). Several probe molecules can be used simultaneously or more commonly in sequence.

Acid sites can be Lewis or Brønsted sites. Coordinatively unsaturated sites (cations) are electron acceptors, and thus Lewis acids. OH groups can give their proton away and are Brønsted sites. Lewis sites will bind to nucleophilic molecules. Brønsted sites will form with the basic probe molecule various types of complexes. Depending on the strength of the site (and of the probe), a weak or strong H-bond can be formed, or even a more or less dissociated ion pair. When the size of the molecule is comparable to that of the oxide cavity, electron densities in the basic molecule are modified, the basicity of the probe can be enhanced, and the proton transfer can occur more easily.

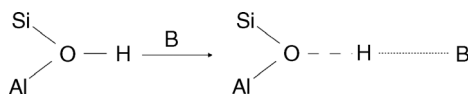


**Figure 1.14** Interaction of a base with a Brønsted site and creation of an H-bond.

All of these parameters show that the basicity of the probe molecule cannot be considered without the solid, and that it is always a pair at work.

#### 1.4.4.1 Brønsted Sites: Hydrogen Bonding and IR Spectroscopy

When a H-bond is created between the probe molecule and a hydroxyl group on the surface (Figure 1.14), the electron density between the oxygen and hydrogen atoms decreases, the distance between them increases, and the OH bonding is weakened. The elongation vibration  $\nu(\text{OH})$  becomes slower, and the corresponding  $\nu(\text{OH})$  band is shifted to lower wavenumbers (red or bathochromic shift). Other modifications are induced by the elongation of the OH bond: the variation of the dipolar moment during the vibration also increases, and the integrated intensity of the  $\nu(\text{OH})$  vibration band increases. For reasons that we will explain later, the  $\nu(\text{OH})$  band also broadens when the proton is engaged in H-bonding, and the maximum intensity decreases (the band “flattens”).

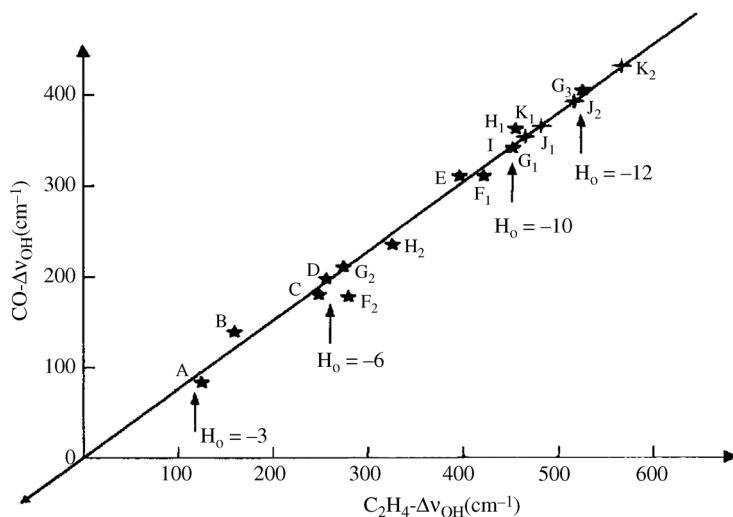
**1.4.4.1.1 Quantification of the  $\nu(\text{OH})$  Shift [20]** The size of the bathochromic shift of the  $\nu(\text{OH})$  band, denoted  $\Delta\nu(\text{OH})$ , is a good measurement for the formation enthalpy for H-bonding (bond strength,  $\Delta H$ ). There is no simple relationship between  $\Delta H$  and  $\Delta\nu(\text{OH})$ , but similarly to the case of cyclohexanol in various solvent,  $\Delta H$  is considered to be proportional to  $\sqrt{\Delta\nu(\text{OH})}$ . A series of bases can be used to build a scale with which acids can be compared. This is the so-called BHW method (Bellamy–Hallam–Williams) (Figure 1.15). In that case, the ratio of  $\Delta\nu(\text{OH})$  to the frequency  $\nu_0$  for the free OH group is preferred. For two acids 1 and 2, the points obtained for the series of bases will fit a straight line:

$$\left(\frac{\Delta\nu}{\nu_0}\right)_1 = A + B\left(\frac{\Delta\nu}{\nu_0}\right)_2$$

where  $B$  is the relative strength of 1 compared with 2.  $B$  can be linked to parameters describing the Brønsted acid strength, such as  $\text{p}K_a$ .

**1.4.4.1.2 Distortion of  $\nu(\text{OH})$**  When an H-bond is created, the width at half-maximum increases considerably for the  $\nu(\text{OH})$  vibration band [22]. This can be explained partly by the deformation of the OH vibrator, because of the interaction between the proton and a second nucleophilic center.

In the extreme case of protonation, the curve of the energy as a function of the O–H interatomic distance (Morse curve) presents two separate minima: one with the proton on the oxygen atom, and the other (deeper) one for the proton transferred on the nucleophilic probe molecule (Figure 1.16). In the case of a moderate interaction, the Morse curve is already far from that of a harmonic oscillator.



- |                                   |   |  |  |
|-----------------------------------|---|--|--|
| ★ A                               | SiO <sub>2</sub>  | ★ G <sub>1</sub> , G <sub>2</sub> , G <sub>3</sub> | HYSA(9.5) (HF, BF, 3600)   |
| ★ B                               | Al <sub>2</sub> O <sub>3</sub>                                | ★ H <sub>1</sub> , H <sub>2</sub>                  | HYSA(37) (HF and BF)   |
| ★ C                               | P <sub>2</sub> O <sub>5</sub> /Al <sub>2</sub> O <sub>3</sub> | ★ I  | ZEOLITEβ   |
| ★ D                               | SiO <sub>2</sub> -Al <sub>2</sub> O <sub>3</sub>              | ★ J <sub>1</sub> , J <sub>2</sub>                  | HY6401N (HF and 3600)  |
| ★ E                               | HY(2.7)   | ★ K <sub>1</sub> , K <sub>2</sub>                  | HY6401N sulfated with V <sub>2</sub> O <sub>5</sub><br>(HF and 3600) |
| ★ F <sub>1</sub> , F <sub>2</sub> | HYI(4.7) (HF and BF)  |  |  |

**Figure 1.15** BHW curve on acid catalysts – acidity scale obtained by comparison of  $\Delta\nu(\text{OH})$  between CO and ethylene. After [21]

A second possible reason for the broadening of the  $\nu(\text{OH})$  band can be the presence of many different acidic hydroxyl groups, in a heterogeneous distribution. In solid acids with a complex structure, a seemingly simple  $\nu(\text{OH})$  band can in fact represent the overlap of many bands due to sites differing slightly in environment and acidity.

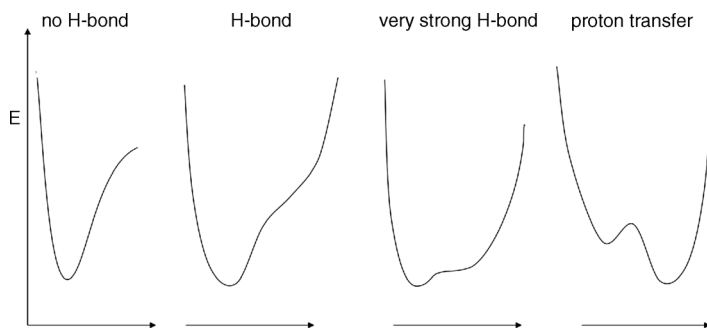


**Figure 1.16** Energy as a function of OH distance in an acidic hydroxy group, in the presence of a probe molecule (Morse function).

Since band shifts can be very different from one to another,  $\nu(\text{OH})_{\text{assoc}}$  for associated OH groups will be a more or less resolved band group whereas  $\nu(\text{OH})_{\text{free}}$  for free OH groups seems like a unique band.

**1.4.4.1.3 Evans' Windows** Fermi resonances can also increase the complex aspect of the spectrum for  $\nu(\text{OH})_{\text{assoc}}$ . Fermi resonances generally arise when the fundamental vibration comes very close to a combination band with the same symmetry. The overlap will not be simple, and both bands seem to reject one another. Both bands will be shifted and the spacing between them will be larger than it should have been without the resonance. When one of the bands is very large [as expected for  $\nu(\text{OH})_{\text{assoc}}$ ] and the other one is narrow, the narrow band will in fact appear like a transmission window in the broad band. The first harmonic of the  $\delta(\text{OH})$  vibration (in-plane deformation of the OH group) coming very close to the  $\nu(\text{OH})_{\text{ass}}$  creates a so-called Evans' window [23–26] (Figure 1.17). This is very typical and indicative of very strong H-bonding. The  $\nu(\text{OH})$  band broadens and shifts to lower wavenumbers, eventually overlapping the two  $\delta(\text{OH})$  and two  $\gamma(\text{OH})$  harmonics, themselves shifted to higher wavenumbers by the H-bonding. The band structure observed is often referred to as an A, B, C system. H-bond strengths for OH bands in A, B, C systems

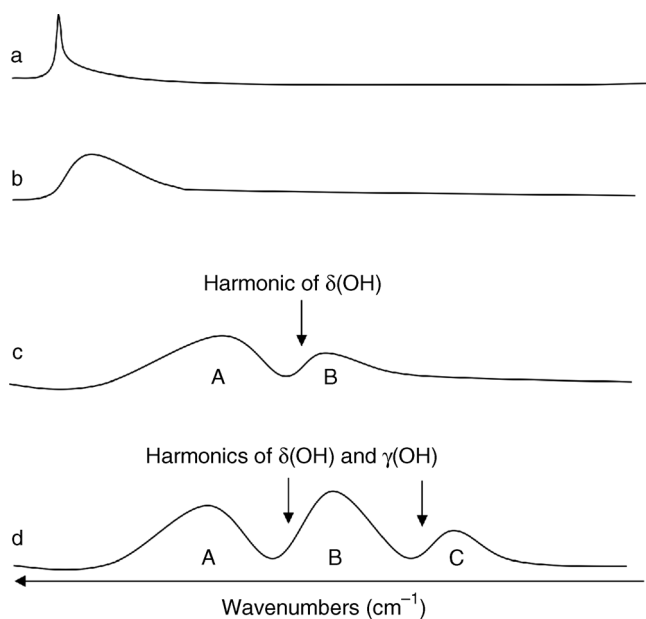


**Figure 1.17** Evans' window on a  $\nu(\text{OH})$  vibration in the case of a strong H-bond: (a) free  $\nu(\text{OH})$ , no H-bond; (b)  $\nu(\text{OH})$  perturbed by a H-bond; (c) strong H-bond, overlap with the first harmonic of the  $\delta(\text{OH})$  deformation

vibration, the AB band system appears (the harmonics themselves are too weak to be observed directly); (d) very strong H-bond, overlap with both the harmonics of  $\delta(\text{OH})$  and  $\gamma(\text{OH})$ , the C band appears.

can be compared by using the wavenumber values of the center of gravity of each band system.

#### 1.4.4.2 Molecular Probes for Lewis Acidity

Lewis acidity is characterized by the absence of any proton at play. No direct observation of any vibration band for the acidic site is possible. It is only by the influence of the site on a probe molecule that IR observation will give information on the Lewis site. Some probe molecules are particularly sensitive to interaction with Lewis sites, and their IR bands can be clearly modified differently by Brønsted and by Lewis sites. These are mostly pyridines, carbon monoxide, nitriles, and ammonia. These probe molecules are described below.

Transformation of a Lewis into a Brønsted site is possible when water or H<sub>2</sub>S is adsorbed on the surface [27–29]. Lewis acidity can be masked, and the acidity is transferred to the proton on the adsorbed molecule, thus showing Brønsted acidity. The reverse is also possible, and a Brønsted site can be transformed into a Lewis site, for example, when alkenes are present on the surface. Alkenes can be protonated by Brønsted sites and form carbenium ions that can be detected with a probe molecule (acetonitrile, for example) while the OH group disappears [30, 31].

#### 1.4.4.3 Common Probe Molecules for Acidity

The most common probes for the characterization of acidity in solids are amines (pyridines, NH<sub>3</sub>), carbon monoxide, nitriles, nitrogen, and oxygen. Any nucleophilic molecule is a base, and the above list is, of course, not exclusive. Many molecules correspond to the criteria for good probe molecules, and benzene, ozone, ketones, alcohols, halogenated alkanes, dioxane, tetrahydrofuran (THF), and dimethyl sulfide (DMSO), for example, have been used.

**1.4.4.3.1 Pyridines** Pyridine is one of the most commonly used probes for the study of solid acids [32–35]. It is easy to use and gives information on the type and amount of sites on the surface. It is a very strong base, protonated on strong Brønsted acid sites (BASs) and coordinated strongly on Lewis acid sites (LASs). With weak BASs such as the silanol group of silica, it can form H-bonds. Three types of complexes can thus be observed on the surface of an oxide: PyH<sup>+</sup>, PyL, and Py–HO (together with physisorbed pseudo-liquid pyridine). All three can be identified by the frequency of the bands from the vibration of the heteroaromatic cycle between 1400 and 1700 cm<sup>-1</sup>. The bands due to the 19b and 8a vibration modes (Table 1.1) are very sensitive to coordination on the nitrogen atom and are used to identify and quantify the sites. The shift of the 8a mode is used to measure the strength of LASs. The spectral region of the  $\nu$ CH(D) vibration is not often used, but it contains interesting information. Both  $\nu$ CH(D) frequency and intensity are sensitive to the adsorption mode and allow one to distinguish between H-bonded, protonated, and coordinated species (Figure 1.18). It was found that the study of  $\nu$ (CH) modes is more reliable than that of the 8a and 19b modes to distinguish H-bonded from weakly coordinated species. An example of such an application was given for the cases of CeO<sub>2</sub>, MgO, and CaO [36].

**Table 1.1** Typical frequencies ( $\text{cm}^{-1}$ ) for adsorption of pyridine on a solid acid<sup>a)</sup>.

	$\nu_{8a}$ $\nu(\text{CC})$	$\nu_{8b}$ $\nu(\text{CC})$	$\nu_{19a}$ $\nu(\text{CN})$	$\nu_{19b}$ $\nu(\text{CN})$
Gas	1584	1580	1483	1440
H-bond	1595	1580	1490 ww	1445
Lewis	1630–1600	1580 ww	1490 ww	1450
Brønsted	1640	1610	1490	1545

a) Data for the gas are given as a reference. ww: very weak band.

Adsorption of pyridine is most easily performed by saturation of the sample and evacuation at increasing temperature. The adsorption is done, after thermal activation of the solid under vacuum, by putting the sample under 1 Torr of pyridine vapor in the cell (the gas line must be isolated and evacuated quickly to avoid pollution of all gaskets and unheated surfaces). On micro- or mesoporous materials, closing the cell and heating the sample at 473 K for a few minutes with the pyridine vapor improves diffusion of the probe inside the solid cavities and insures a correct interaction with the adsorption sites. The cell is then evacuated at the same temperature (before cooling) in order to remove all physisorbed pyridine. On strongly adsorbing solids, such as zeolites, a high temperature (473 K) is needed to obtain clear and unambiguous spectra. It should be noted that at high pyridine coverage, protonated pyridine dimers can sometimes be formed. For weakly acidic solids, a progressive thermodesorption can be tried instead of direct evacuation at 473 K, but the measure of real (strong) BASs is only valid after desorption under vacuum at high temperature.

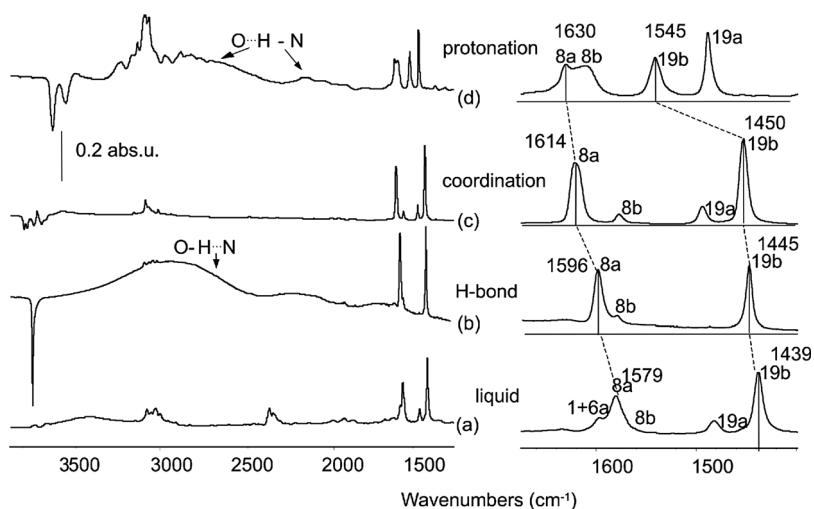


**Figure 1.18** Spectra for pyridine in the  $1400\text{--}4000\text{ cm}^{-1}$  region: (a) in the liquid phase; (b) after adsorption on silica and evacuation at room temperature; (c) on alumina, with evacuation at  $100\text{ }^{\circ}\text{C}$ ; (d) on HY at  $200\text{ }^{\circ}\text{C}$ . Spectra by A. Vimont.

Molar absorption coefficients given in the literature can be used for quantitative measurements. The bands of interest must be integrated and the area multiplied by the value of the coefficient to determine the amount of pyridine on the surface, and thus the number of sites (to be divided by the sample weight and by the surface of the water to calculate the number of sites per gram). Typical values are  $\epsilon_{1545}(\text{pyH}^+) = 1.3 \mu\text{mol}^{-1} \text{cm}$  for Brønsted sites and  $\epsilon_{1450}(\text{pyL}) = 1.5\text{--}2 \mu\text{mol}^{-1} \text{cm}$  for Lewis sites. The values measured for  $\epsilon$  by various authors can be very different. The temperature of the desorption of physisorbed pyridine or the adsorption of a significant amount of the probe on the cell walls might be the reason for this. In a combined IR–gravimetric experiment, the need for a temperature as high as 473 K was shown, and the value of  $\epsilon_{1545}(\text{pyH}^+) = 1.36 \pm 0.03 \mu\text{mol}^{-1} \text{cm}$  was confirmed on an H–Y zeolite. These absorption coefficients are considered to be valid for one given solid only, however, and results obtained in that way must be considered as a first approximation.

**1.4.4.3.2 Substituted Pyridines** 2,6-Dimethylpyridine (DMP or lutidine) can be more convenient than pyridine to detect weak Brønsted acidity due to its higher basicity ( $\text{p}K_{\text{a}} = 6.7$  compared with 5.2 for pyridine) [37–39]. As an example, no Brønsted acid sites were detected by pyridine adsorption on  $\text{TiO}_2\text{--ZrO}_2$  mixed oxides whereas, under the same conditions, the formation of protonated species was observed by adsorption of DMP [40]. Spectral features in the  $1660\text{--}1550 \text{ cm}^{-1}$  range ( $\nu_{8\text{a}}$  and  $\nu_{8\text{b}}$  vibrations) account for the different adsorption modes of DMP with the solid surface (Table 1.2) [41]. Another advantage of this probe compared with pyridine is its ability to give information on Brønsted acid strength (Figure 1.19). The positions of  $\nu_{8\text{a}}$  and  $\nu^*(\text{NH})$  bands in the spectrum of protonated DMP vary with the strength of Brønsted acidity: the higher the  $\nu^*(\text{NH})$  wavenumber and the lower the  $\nu_{8\text{a}}$  wavenumber, the stronger is the acidity. On a series of zeolites, it was shown that the ranking obtained with DMP adsorption is correlated with that obtained by CO adsorption. On tungsten oxide or niobium oxide supported on titania, the determination of molar absorption coefficient of protonated DMP [ $\epsilon(\nu_{8\text{a}} + \nu_{8\text{b}}) \approx 6.8 \mu\text{mol}^{-1} \text{cm}$ ] allowed the quantification of both strong and medium Brønsted acid sites [42].

Substituted pyridines are also used as Brønsted-specific probes, especially in zeolites. Access of the nitrogen atom to the acid site is hindered by the neighboring substituents. Since the proton in Brønsted sites protrudes from the surface of the solid (in contrast to electronic vacancies on Lewis sites), DMP and collidine interact

**Table 1.2** Typical frequencies ( $\text{cm}^{-1}$ ) for 2,6-dimethylpyridine according to its adsorption modes.

	$\nu_{8\text{a}}$ $\nu(\text{CC})$	$\nu_{8\text{b}}$ $\nu(\text{CC})$	$\nu_{19\text{a}}$ $\nu(\text{CN})$	$\nu_{19\text{b}}$ $\nu(\text{CN})$
Gas	1584	1580	1480	1410
H-bond	$\sim 1602$	1580	1480	1410
Lewis	1595–1620	1580	1477	1410
Brønsted	1640–1655	1630	1473	1415

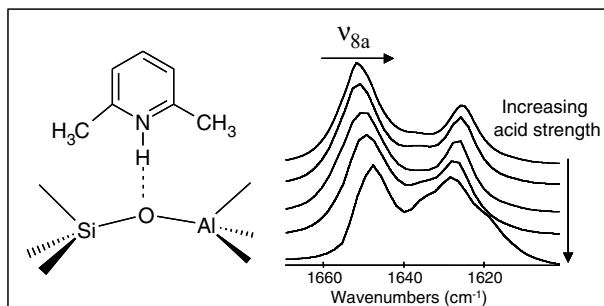


**Figure 1.19** Spectra in the  $1600\text{--}1700\text{ cm}^{-1}$  region for DMP protonated on different zeolites [from top to bottom: LiHNaY, KHNaY, HY(2.9), HNaX, HYSA]. From [41]

more easily with Brønsted than with Lewis sites, and some selectivity can be observed. Steric hindrance around Brønsted sites can also decrease the interaction with the basic probe, and the H-bond can be weaker than with an unsubstituted pyridine. Great care must be taken in the use of these probes.

**1.4.4.3.3 Accessibility of Sites** To be active in a catalytic reaction, a surface site must be accessible to reactants and products. An accessibility index (ACI) was derived from IR spectroscopy of substituted alkyipyridines with different sizes (pyridine 0.57, DMP 0.67, and collidine 0.74 nm) over hierarchical ZSM-5 crystals. The samples were prepared by selective silicon extraction of a parent commercial sample in alkaline medium (desilication) and contained different degrees of intracrystalline mesoporosity. The enhanced accessibility of acid sites in the hierarchical zeolites was shown. A relatively bulky molecule such as collidine, which probes practically no acid site in the parent medium-pore MFI structure, can access up to 40% of the Brønsted sites in the mesoporous sample. The ACI is a powerful tool to standardize acid site accessibility in zeolites and can be used to rank the effectiveness of synthetic strategies towards hierarchical zeolites (mesoporous crystals, nanocrystals, and composites) [43].

**1.4.4.3.4 Carbon Monoxide** Carbon monoxide is also very important a probe molecule [44–47]. It is a weak base, which is not protonated but can perturb the proton by interaction with the carbon atom in the molecule. Since the interaction is often weak with acid sites, the adsorption must be performed at low temperature (100 K in a liquid nitrogen-cooled cell) (Figure 1.20). The frequency of the  $\nu(\text{CO})$  vibration band is very sensitive to coordination and can shift from  $2138\text{ cm}^{-1}$  (starting position, pseudo-liquid CO at 100 K on the surface) up to  $2170\text{ cm}^{-1}$  on Brønsted sites and  $2240\text{ cm}^{-1}$  for strong Lewis sites (Table 1.3). At the same time, on Brønsted sites, H-bonding between CO and the proton induces a large red shift of the  $\nu(\text{OH})$  vibration band. A clear relationship has been shown between the  $\Delta\nu(\text{OH})$  shift and the position of the  $\nu(\text{CO})$  frequency, showing the quality of the scale obtained for ranking solid acids with this probe molecule (Figure 1.21). It should be noted that the frequency of the  $\nu(\text{CO})$  band is influenced by the coverage level, and that the value must be extrapolated to zero coverage by performing a progressive adsorption [48].

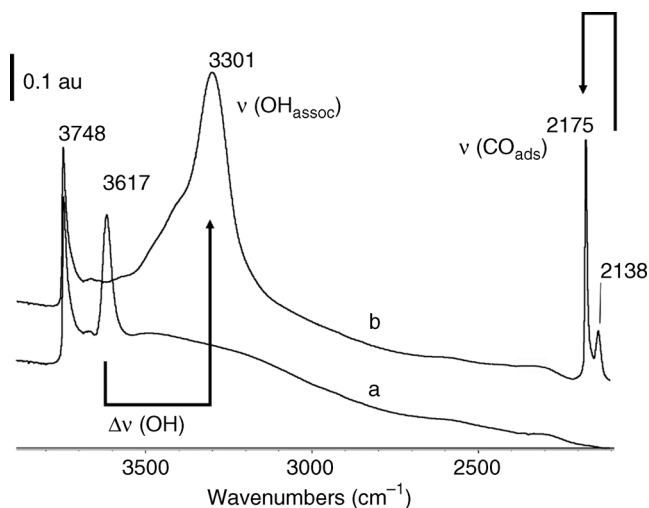


**Figure 1.20** Spectrum of an H-ZSM5 zeolite (a) before and (b) after adsorption of CO at 100 K.

Carbon monoxide can be used quantitatively for measuring the number of sites. By progressive introduction of known amounts of the probe molecule (a few milliliters under a few millibars pressure, all accurately measured) inside the cell, the amount of CO introduced when saturation is reached and the molar absorptance coefficient can be determined accurately (Figure 1.22). A typical value for the molar absorptance coefficient on Brønsted sites is  $\epsilon\nu(\text{CO}) = 2.7 \text{ cm } \mu\text{mol}^{-1}$ .

Carbon monoxide is also an excellent probe molecule for metals and sulfides, and this is detailed in the relevant sections.

**1.4.4.3.5 Pyridine–CO Coadsorption** Successive coadsorption of pyridine(s) and CO allows the measurement of acidity in various environments on the same catalyst. This is especially true for zeolites. Mordenite, for example, if activated with great care, contains Brønsted sites which are not accessible to pyridine in the side pockets of the structure. Sites located in the large channels can therefore be perturbed by the initial introduction of pyridine in the pore system. Adsorption of CO in a second step will only reach OH acid sites which are out of reach of pyridine, in the small side pockets. The response measured after CO adsorption will give a measurement of the amount

**Table 1.3** Typical frequencies ( $\text{cm}^{-1}$ ) for bands after CO adsorption.

	Silanol groups	Brønsted sites	Lewis sites
$\nu(\text{CO})$	$\sim 2150$	2155–2180	2190–2240
$\Delta\nu(\text{CO})$	$\sim 15$	20–45	50–100
$\Delta\nu(\text{OH})$	$\sim 90$	100–400	

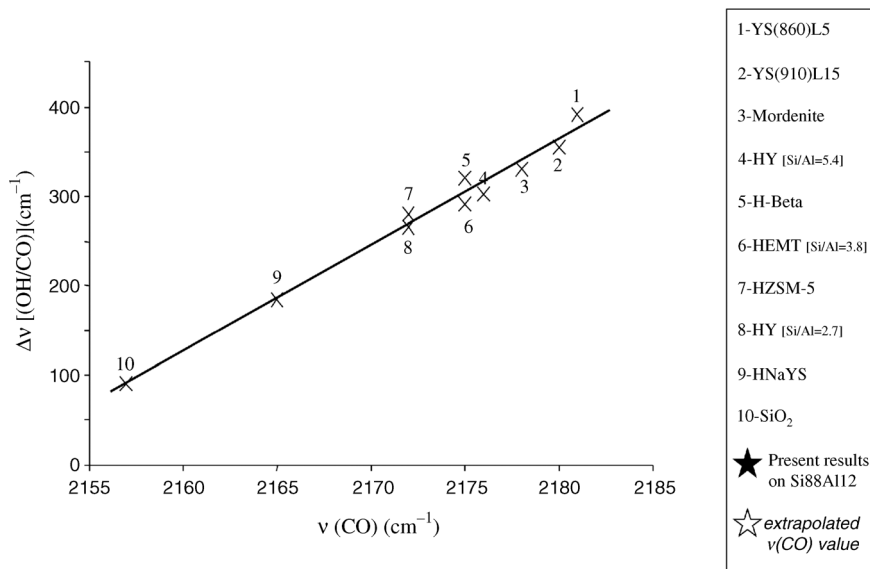


**Figure 1.21**  $\Delta\nu(\text{OH})$  and the corresponding  $\nu(\text{CO})$  for various acidic solids and zeolites. . From [13]

and strength of sites in the side pockets, which can be compared with the situation in the absence of pyridine, when all sites are probed by CO. The sites in the side-pockets were measured as slightly weaker than in the main channels, and represented one-third of the total amount [11, 49]. The same was done in dealuminated mordenites, and pyridines with increasing size were used to show the increase in accessibility in the pores of mordenite after dealumination. Even di-*tert*-butylpyridine was able to probe Brønsted sites in the dealuminated mordenite, thus showing that the pore structure was largely modified [50, 51].

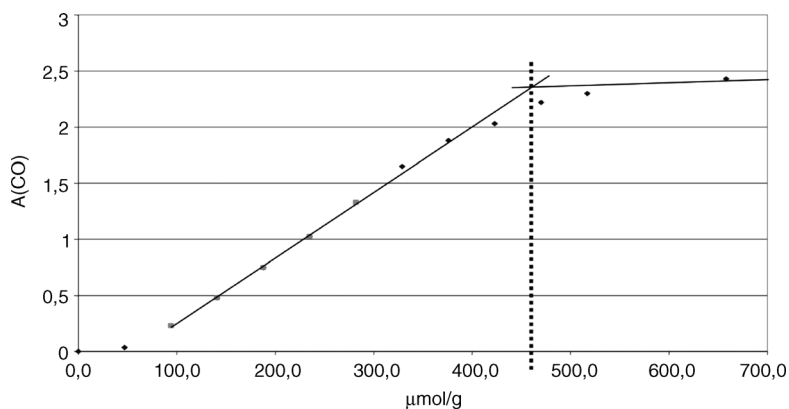


**Figure 1.22** Determination of the amount of surface sites on a solid by progressive introduction of CO in controlled amounts inside the cell.

**1.4.4.3.6 Acetonitrile** Acetonitrile is a stronger base than CO [52–54]. It can be adsorbed at room temperature on Lewis and Brønsted sites in oxides. It is a small molecule, and it can access most of the acid sites (Table 1.4). Its fairly strong basicity makes it very interesting, since it is the probe that forms the strongest possible H-bond with Brønsted sites before the proton is actually transferred: it is with acetonitrile that the strongest H-bond is formed, and the largest  $\Delta\nu(\text{OH})$  is observed. Acetonitrile can be protonated, but only by acids at the limit of superacidity [55], or by very strong acid sites upon heating. Protonation of acetonitrile can also be produced by strong confinement by acidic sites in some zeolite pores. The protonation temperature of acetonitrile has been used to build a scale for acidity, producing a ranking of acidic catalysts in agreement with results in saturated hydrocarbon conversion at high temperature. The transfer of the proton from the zeolite to acetonitrile occurs only at high temperature, and that temperature is a good indication of the difficulty of the catalytic proton transfer from the solid acid to the hydrocarbon, which is the initial step of the conversion of saturated hydrocarbons on acidic zeolites. This measurement takes into account the influence of confinement on the proton transfer. It is in fact the only probe molecule acidity scale agreeing with catalysis results for demanding reactions [56].

One of the main difficulties with acetonitrile is the presence of many Fermi resonances in the spectrum. The  $\nu(\text{CN})$  vibration in adsorbed  $\text{CH}_3\text{CN}$  is split into a doublet because of interaction between the vibrations of the CH and CN groups. This is avoided by using  $\text{CD}_3\text{CN}$  instead of  $\text{CH}_3\text{CN}$ . The  $\nu(\text{C}\equiv\text{N})$  is fairly sensitive to molecular interactions, and shifts up to  $2330\text{ cm}^{-1}$  on strong Lewis sites (Table 1.4).

The very strong H-bond formed on Brønsted sites also produces a very typical shift of the  $\nu(\text{OH})$  band, with Evan's windows as described earlier (Figure 1.23). The value of  $\Delta\nu(\text{OH})$  can be estimated by the position of the center of gravity of the A, B (C) system, allowing a close comparison of Brønsted sites in various solids. This is a very strong point for using deuterated acetonitrile rather than pyridine for measuring the strength of Brønsted acid sites.

**1.4.4.3.7 Ammonia** Simple and aliphatic amines are strong bases, and can be (rather complex) probe molecules. They can form many different adsorbed species, interacting with both Lewis and Brønsted sites, by autoassociation and protonation, and they can also interact with basic sites [57]. The autoassociation of the base can lead to the formation of new complexes with hydroxy groups and to the broadening of the  $\nu(\text{OH})_{\text{assoc}}$  band, which can sometimes disappear completely. Ammonia itself is a

**Table 1.4** Typical frequencies ( $\text{cm}^{-1}$ ) for the various states of adsorbed acetonitrile.

	Physisorption	Silanol groups	Brønsted sites	Protonation	Lewis sites
$\nu(\text{C}\equiv\text{N})$	2245	$\sim 2285$	2295–2300	2310–2320	2325–2330
$\Delta\nu(\text{C}\equiv\text{N})$	0	$\sim 40$	50–55	$\sim 70$	$\sim 85$
$\Delta\nu(\text{OH})$	0	$\sim 300$	500–1000	—	—

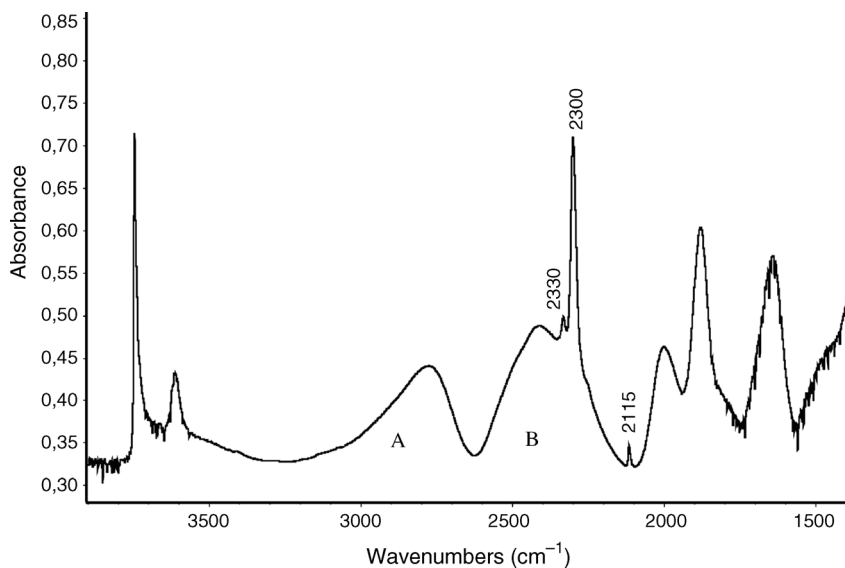


**Figure 1.23** Spectrum of H-ZSM5 after adsorption of  $\text{CD}_3\text{CN}$  at room temperature, in such an amount as not to saturate all acidic sites. The A, B system and the Evans' window are clearly visible, and also the  $\nu(\text{C}\equiv\text{N})$  band

due to adsorption on Lewis sites at  $2330\text{ cm}^{-1}$  and on Brønsted sites at  $2300\text{ cm}^{-1}$ . The band at  $2115\text{ cm}^{-1}$  is due to the vibration of the  $\text{CD}_3$  group.

particularly strong base, with a very small size, and it will reach all acid sites on a solid. The various types of adsorbed ammonia, protonated or not, can be distinguished in the IR spectrum (Figure 1.24, Table 1.5).

Dissociative adsorption of ammonia has also been observed ( $\text{NH}_3/\text{NH}_2^-$   $\text{p}K_a = 38$ ), and the strong basicity of the probe makes it not very specific. Many IR studies have shown that ammonia adsorption is a very complex phenomenon, and its use is not recommended.

Aliphatic amines are also not much used because of their even stronger basicity and lower specificity. They are reactive molecules and can also give a proton away. Quantitative measurements are difficult because the amount of adsorbed amine depends more on the "area" of the molecule itself than on its interaction with the acid site.

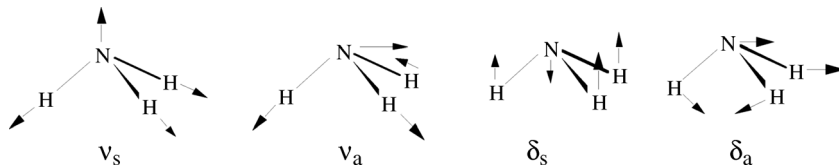


**Figure 1.24** Vibrations in the ammonia molecule.

**Table 1.5** Typical frequencies ( $\text{cm}^{-1}$ ) observed upon adsorption of  $\text{NH}_3$  on a solid acid<sup>a)</sup>.

	va	vs	$\delta_a$	$\delta_s$
Gas	3444	3336	1628	950
H-bond	3408	3309	1625	1036
Lewis:				
ZrO <sub>2</sub>	3380	3280	1610	1230–1190
ZnO	3420–3350		1630	1220
Al <sub>2</sub> O <sub>3</sub>	3400	3270	1620	1280–1240
NH <sub>3</sub> -BF <sub>3</sub>	3343	3279	1599	1438
Strong Brønsted: NH <sub>4</sub> <sup>+</sup>	3145 ( $\nu_3$ )	3040 ( $\nu_1$ ) (R)	1680 ( $\nu_2$ ) (R)	1400 ( $\nu_4$ )

a) Data for the gas are reported as a reference. (R) indicates a band active only in Raman spectroscopy.

**1.4.4.3.8 Other Main Probe Molecules for Acid Sites** Homonuclear diatomic molecules, such as hydrogen, nitrogen, and oxygen, are normally not detected in IR spectroscopy. They can, however, be adsorbed on the surface of catalysts at low temperature, and are deformed (polarized) by such adsorption. These molecules then lose their symmetry and become IR active. The local electric field (adsorbing cation) influences the frequency of the vibration band of the molecule, and nitrogen has been used, for example, for characterizing cations and acidic protons in mordenite. One of the main advantages of these diatomic probes is the invisibility of the gas phase, which does not interfere with the quality of the spectra. Nitrogen is a very weak base; it interacts weakly with the sites and allows a very fine differentiation of acid strengths.

Benzene is another weak base interacting with the protons via its  $\pi$ -electron cloud. It allows a fine scaling of acid sites differing only slightly in strength, but the assignment of the various possible types of interactions can be difficult. Benzene can suffer from important steric restraints, and it has been reported not to reach many hindered sites.

## 1.4.5

### Characterization of Basicity with Probe Molecules

Acidic probe molecules can be used for the characterization of basic catalysts. This is very similar to the characterization of acidic sites by basic probe molecules, but the interaction is often much more complex and the acidic probe molecule more reactive. The literature on the topic is not as rich as for acidity, although a few review papers have been published [58, 59].

#### 1.4.5.1 CO<sub>2</sub> as a Probe for Basic Sites

Carbon dioxide is the most commonly used probe molecule for characterizing basic sites. As described earlier, CO<sub>2</sub> either reacts with basic hydroxy groups and forms surface hydrogencarbonates or it reacts with oxygen anions and forms carbonates. Various structures of carbonate species can be formed depending on the various environments of basic sites. The formation of hydrogencarbonates reveals the basic

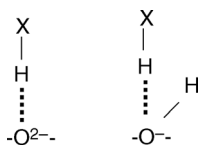


**Figure 1.25** Interaction modes of an acidic protic molecule (XH) with basic centers.

properties of very high-frequency OH groups with bands around  $3780\text{ cm}^{-1}$  on beta-zeolites that correspond to basic OH groups attached to Lewis acidic Al atoms [60]. Comparing the intensity of bands specific to hydrogencarbonate species on various oxides is a way to rank their basic properties and to predict their activity toward COS hydrolysis [61]. However,  $\text{CO}_2$  is not a good probe for assessing the basic strength and quantification of the basic sites is not direct with  $\text{CO}_2$ .

#### 1.4.5.2 Protic Molecules

Adsorption of acidic protic molecules such as acetylene, propyne (methylacetylene), butyne (ethylacetylene), pyrrole ( $\text{C}_4\text{H}_5\text{N}$ ), and chloroform ( $\text{CHCl}_3$ ) is an interesting way to probe the basic strength of surface sites. Indeed, the  $\nu(\text{X-H})$  shift ( $\text{X} = \text{C}$  or  $\text{N}$ ) that is observed after H-bonding of the probe with the surface is a good indicator of the basic strength of the sites (Figure 1.25). However, determining the nature of the basic sites is not easy with this method. These probes tend to decompose and to modify the catalyst surface properties. Hence weakly reactive molecules will be preferred.

Pyrrole, containing an NH moiety, can form H-bonds with basic oxygen atoms on oxides and zeolites. The  $\nu(\text{NH})$  vibration band is shifted, and the value of the shift,  $\Delta\nu(\text{NH})$ , accounts for the strength of the H-bond. If formation of pyrrolate ions occurs, it prevents the assessment of basicity.

Similarly, the extent of the  $\nu(\text{CH})$  band shift of H-bonded chloroform accounts for the strength of the basic sites. However, dissociation of chloroform on acid–base sites contaminates the surface with chlorine ions.

Propyne and acetylene are interesting probes forming H-bonds between the acidic  $\equiv\text{CH}$  groups and the basic sites. On strongly basic oxides such as MgO, a shift of the  $\nu(\equiv\text{CH})$  vibration of propyne from  $3334\text{ cm}^{-1}$  in the gas phase down to  $\sim 3255\text{ cm}^{-1}$  can be observed. Note that propyne can also interact with acidic sites, and forms complexes via its  $\text{C}\equiv\text{C}$  bond with the weakly acidic silanol groups on silica. Propyne is generally preferred over butyne, which polymerizes more easily.

#### 1.4.5.3 Methanol

Methanol, the simplest alcohol molecule, is widely used to characterize basic oxides such as MgO,  $\text{ThO}_2$ ,  $\text{CeO}_2$ , and  $\text{ZrO}_2$  [62–67]. The adsorption modes of methanol, that is, the dissociative adsorption that leads to the formation of hydroxyl and methoxy groups and molecular adsorption, can be discriminated by IR spectroscopy (Figure 1.26). On MgO, the three  $\nu(\text{OC})$  bands observed at about 1115, 1090, and  $1065\text{ cm}^{-1}$  are assigned to the two types of dissociated methanol corresponding to

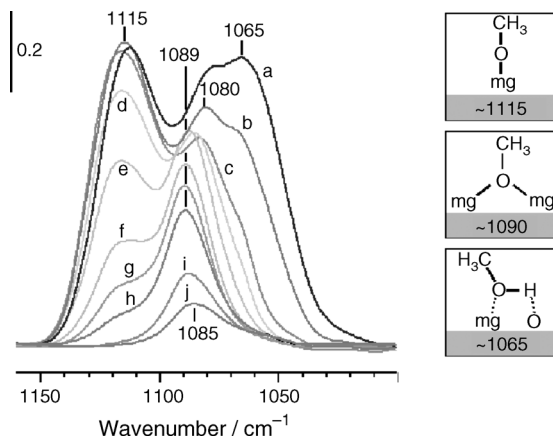


**Figure 1.26** IR spectra of methanol introduced at room temperature on MgO activated at 1023 K, followed by evacuation at (a) room temperature, (b) 348, (c) 398, (d) 448, (e) 498, (f) 548, (g) 598, (h) 648, (i) 698, and (j) 723 K from [66].

linear and bridged methoxy species and to undissociated methanol, respectively. According to DFT calculations, dissociation occurs on surface defects and the formation of these two types of methoxy species can be related to the surface topology, that is, convex and concaves zones of the surface leading to linear and bridged methoxy group formation, respectively [67–69].

By coupling IR spectroscopy with volumetric or thermogravimetric measurements, the molar absorption coefficients of  $\nu(\text{OC})$  vibration of the various forms of adsorbed methanol could be accurately determined (for MgO,  $\epsilon_{\text{undissociated}} = 2.5 \mu\text{mol}^{-1} \text{cm}$ ;  $\epsilon_{\text{I}} = \epsilon_{\text{II}} = 6.1 \mu\text{mol}^{-1} \text{cm}$ ) (Figure 1.27). Thanks to these results, IR spectroscopy becomes the only method that allows one both to discriminate and to quantify the defects on complex surfaces such as that of MgO, in terms of concentrations of convex and concave defective zones.

#### 1.4.6

#### Probes for Supported Metal Catalysts

IR spectroscopy is a powerful technique to study the adsorption of molecules on well-defined metal surfaces and also on metals supported on oxides. For metal characterization, NO can be used as a probe molecule [70], but CO is the most frequently used probe, and a number of reviews on CO adsorption on metals are available [46, 71–73]. The advantage of CO is the high absorption coefficient of the  $\nu(\text{CO})$  mode and the high sensitivity of its frequency to the oxidation state of the site, to its geometry and to its coordinative unsaturation degree. The (strong) chemical bond between CO and the metal involves electron donation from the  $5\sigma$  orbital of CO to the metal and back-donation from metal d orbitals into the empty  $2\pi^*$  antibonding orbital of CO. Since the  $5\sigma$  orbital is weakly anti bonding and the  $2\pi^*$  orbital is strongly antibonding,

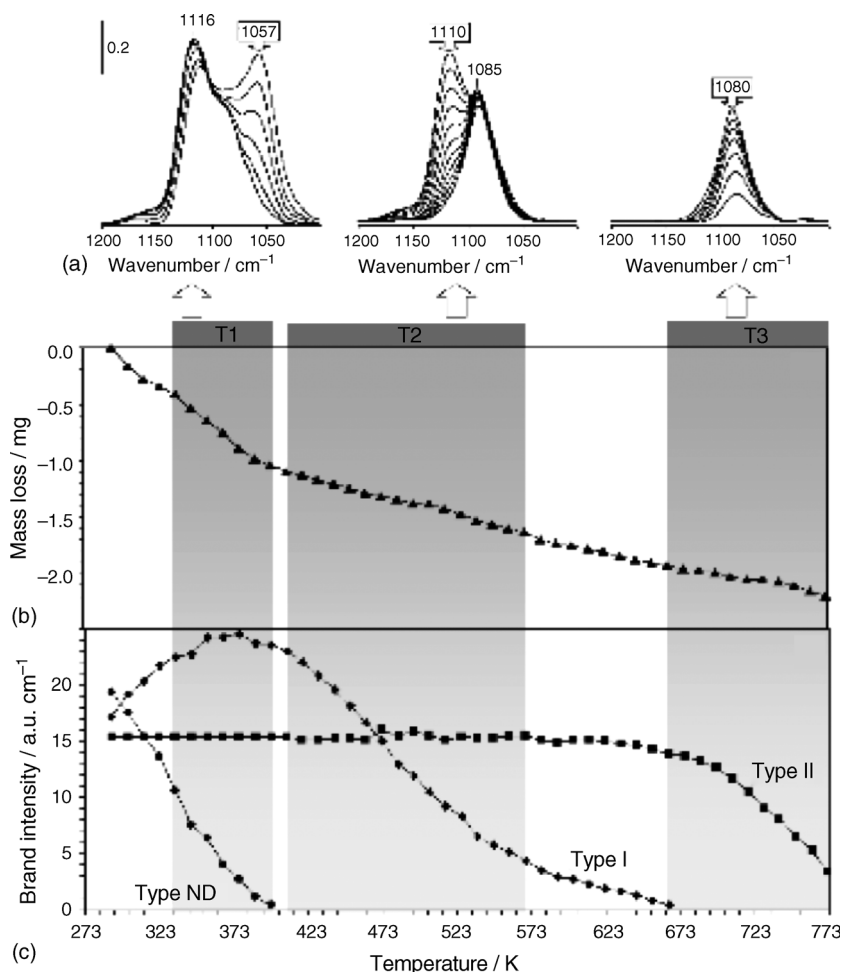


**Figure 1.27** (a) Infrared spectral changes, (b) mass loss, and (c) decrease in methanol  $\nu(\text{OC})$  band areas versus the temperature of methanol desorption on P-MgO measured on

the coupled IR–thermogravimetry setup. T1, T2 and T3: characteristic temperature zones of methanol desorption. From [66].

the C–O bond is weakened by the chemisorption process. Therefore, the increase in the amount of back-donation into the  $2\pi^*$  orbital leads to a decrease in the C–O stretching frequency. Hence the  $\nu(\text{CO}/\text{metal})$  signal appears at lower wavenumbers than that of the gas phase ( $2143 \text{ cm}^{-1}$ ). For spectral interpretation, it is important to take into account the dipolar coupling effects which induce marked wavenumber shifts and intensity transfers. By following frequency shifts for various coverages, bandwidths, and intensities, CO allows one to specify whether the probe molecule forms islands or is well dispersed on the surface. In addition, using IR spectroscopy

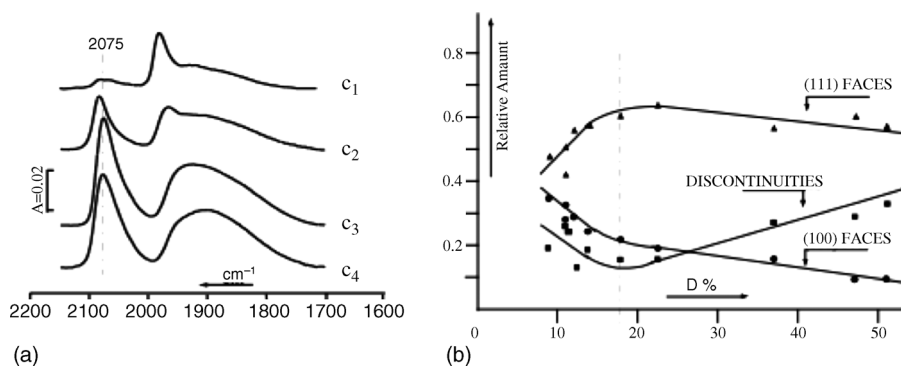


**Figure 1.28** (a) Comparison of CO adsorption for saturation dose, on Pd/Al<sub>2</sub>O<sub>3</sub> reduced at 373 K presenting various dispersions ( $c_1 < c_2 < c_3 \approx c_4$ ). (b) Relative amount of faces and discontinuities versus the dispersion. From [74]

coupled with volumetric measurements, the amount of CO adsorbed on metal sites can be determined, allowing one to calculate the dispersion of the metal particles. In their earlier work [74], Binet *et al.* showed that on an alumina-supported Pd catalyst, changing the dispersion of metallic particles leads to modification of preferentially exposed metallic phase (Figure 1.28).

#### 1.4.7

#### Probes for Sulfide Catalysts

Hydrotreatment is a key process in refineries that aims at reducing the heteroatom content (sulfur, nitrogen, and metals) of petroleum feedstock. The active phases of hydrotreating catalysts generally consist of nanosized mixed sulfide particles (Co–Mo–S or Ni–Mo–S or equivalent with W) supported on alumina-based oxides or more acidic oxides.

Sulfided catalysts are extremely sensitive to oxygen contact. Therefore, characterization of their surface sites requires *in situ* sulfidation, generally performed by heating the oxidic catalyst at atmospheric pressure under a flow of H<sub>2</sub>–H<sub>2</sub>S. Only a few papers have reported IR characterization after sulfidation in conditions close to the industrial ones, such as under a high pressure of H<sub>2</sub>S–H<sub>2</sub> [75, 76] or under a liquid phase. Note that sulfided samples show a very high absorbance towards the IR beam, which makes their analysis difficult.

Nitrogen monoxide is the most commonly employed probe molecule for sulfide catalyst characterization since it has the advantage of being strongly adsorbed on the sulfide phase [77]. However, partial oxidation of the sulfide phase may occur, even at very low temperatures, which could explain the many disagreements found in the literature on IR observations of NO adsorbed on sulfide catalysts.

CO is very informative in characterizing sulfide catalysts and no undesired reaction between the sulfide phase and CO occurs if the adsorption is performed at low temperature (~100 K) [78–80]. On unpromoted sulfide Mo catalyst, a  $\nu(\text{CO})$

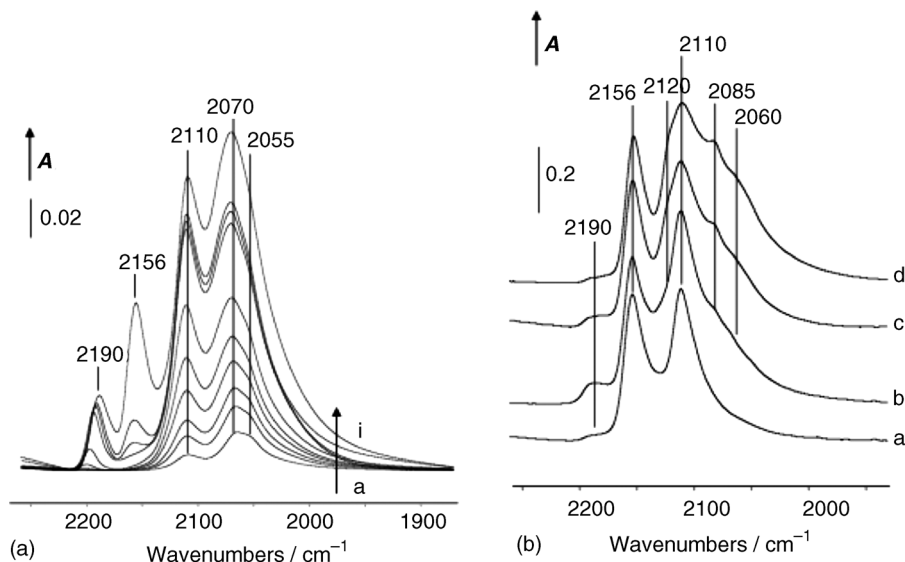


**Figure 1.29** IR spectra of CO adsorbed (100 K) on (a) sulfided CoMo/Al<sub>2</sub>O<sub>3</sub> catalyst (3.2 wt% Co–8.7% Mo). Spectra a–i: increasing CO doses. (b) On sulfided (Ni)Mo/Al<sub>2</sub>O<sub>3</sub> catalysts.

Spectrum a: Mo/Al<sub>2</sub>O<sub>3</sub> (8.7% Mo); Spectra b, c, and d: NiMo/Al<sub>2</sub>O<sub>3</sub> containing 0.5, 1.5, and 3.4 wt% Ni, respectively (133 Pa of CO). From [78].

band at 2110 cm<sup>-1</sup> is detected that characterizes edge sites of MoS<sub>2</sub> slabs. With the CoMo system, as expected, the band at 2110 cm<sup>-1</sup> is decreased (but generally still present) while a band at 2070 cm<sup>-1</sup> specific to the promotion by Co appears (Figure 1.29). It is assigned to CO interacting either with a Co atom or with a Mo atom adjacent to a Co atom. With the NiMo system, CO adsorption on Ni centers of the promoted phase leads to high wavenumber band at ~2120 cm<sup>-1</sup> that strongly overlap the band at 2110 cm<sup>-1</sup> characteristic of non-promoted Mo sites. For NiMo and CoMo catalysts, broad shoulders at low wavenumbers (below 2060 cm<sup>-1</sup>) are characteristic of Mo centers adjacent to promoter atoms, indicating partial decoration of the MoS<sub>2</sub> edges by the promoter. Hence CO characterizes the nature [unpromoted Mo, Co, or Ni-promoted Mo (W) sites], the environment, and the amount of sulfide sites. It is a unique tool to account for the degree of promotion of the sulfide slabs. A good correlation could be established between the degree of promotion of a catalyst and its hydrodesulfurization activity (Figure 1.30).

In addition, CO informs on the fraction of support sites not covered by the sulfide phase. Thus, CO characterizes the nature, the strength, and the number (allowing calculation of the degree of coverage) of accessible acidic sites of the support. A relationship between the acidity of the support and electronic properties of the sulfide phase was evidenced, revealing that the turnover frequency of sulfide sites can be modified by acidic properties of the support.

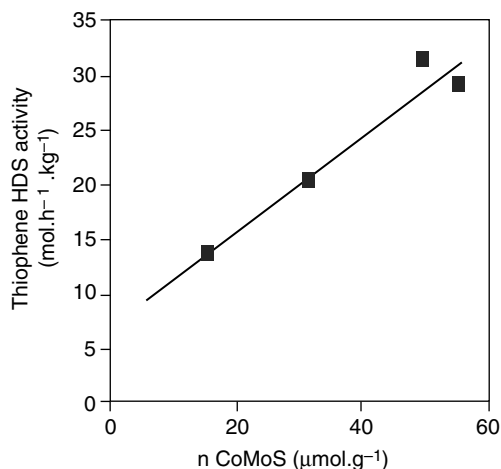


**Figure 1.30** Comparison between the concentration of CoMoS sites and detected by CO (100 K) and their thiophene HDS activity on various NTA-CoMo/ $\text{Al}_2\text{O}_3$  catalysts sulfided at 623 K. From [80].

#### 1.4.8

#### Quantitative Analysis by Coupling IR Spectroscopy with Gravimetry

Quantification of IR data is a key point that generally requires the determination of molar absorption coefficients. Molar absorption coefficients can be measured by progressively adsorbing measured amounts of the probe molecule, and the reader is directed to publications for such advanced measurements [35, 81]. However, even for classical probe molecules such as pyridine, the discrepancies between the values reported in the literature are worth noting. This is likely mainly due to a lack of precise control of the amount of probe adsorbed on the sample. One way to overcome this problem is to couple IR spectroscopy and gravimetric analysis.

Thermogravimetric analysis (TGA) allows weight changes in the sample to be monitored. It has been combined with IR spectroscopy to give reliable quantitative information. It was used to determine the molar absorption coefficients for IR bands of OH groups on silica and HY zeolites, and also for adsorbed probe molecules [82]. Important information was obtained on the quantity of OH groups located in the different cages of HY zeolite and also on the quantity of inner and surface silanol groups on silica. The number of silanol groups accessible to water molecules was shown to be constant whatever the sample of precipitated silica, and also the ratio of water to silanol groups under room atmosphere. Even in the complex cases where several coadsorbed species are formed simultaneously, the molar absorption coefficients could be determined with good accuracy using this setup. An example was presented for methanol adsorption on MgO in Figure 1.27 [66].

Combined TGA and IR spectroscopy was also applied to operando conditions, and denoted AGIR (analysis by gravimetry and infrared) [83]: a modified microbalance was used to follow mass changes (microgram accuracy) inside a catalytic reactor

equipped with IR windows. The spectroscopic response of water and ammonium ions coadsorbed together on zeolites was shown to vary depending on the conditions. The molar absorption coefficients for  $\delta(\text{H}_2\text{O})$  and  $\delta(\text{NH}_4^+)$  at 1640 and 1540  $\text{cm}^{-1}$  for water and ammonia on an HY zeolite were studied under a dry gas flow at various temperatures. The results showed the influence of coverage on the IR response of adsorbed species in zeolites. Adsorption sites change with coverage, bands are shifted and their shape and intensity are modified. Other interesting facts were observed: water modifies strongly the aspect of the  $\delta(\text{NH}_4^+)$  vibration band in ammoniated zeolites, without changing the absorption coefficient. Measuring the sample mass while at the same time recording its IR spectrum showed the key importance of conditions under which the measurements are made. The presence of coadsorbed species (water in particular) strongly modifies the spectrum of surface species. Under reaction conditions, this new technique is especially important for a correct assignment of IR features and catalytic behavior [83].

## 1.5

### Application to Surface Reactivity: Operando Spectroscopy

Owing to its ease of use and its efficiency, IR spectroscopy is one of the most commonly used techniques for studying the surface of a catalyst during a chemical reaction. In 2002, a new term (*operando* spectroscopy) was coined to describe the IR monitoring of the surface under real reaction conditions [84]. The term *in situ*, which was commonly used previously, was more ambiguous and described a measurement which was made in the same place where the reaction was performed (which is the exact meaning of the Latin *in situ*), but not necessarily during the surface reaction. In order to be sure that a study deals with a working catalyst, under meaningful conditions, the word *operando* can only be used when the spectroscopic measurement is combined with a measurement of the catalytic activity by on-line analysis of the reaction products. In this way, changes in the nature and concentration of surface species can be related to catalyst activity and selectivity. The surface of the catalyst under working conditions can be very different from the surface of the activated fresh catalyst under vacuum, and observing the working catalyst under real reaction conditions is critical.

*Operando* IR spectroscopy has progressed considerably since its origin. In 1991, volume 9 of *Catalysis Today* grouped 28 papers after a meeting on “*in situ* methods in catalysis” in the United Kingdom. Of these 28 contributions, 10 dealt with *operando* IR spectroscopy and gave state-of-the-art perspectives. The technique was reaching maturity, but the observed phenomena were complex and conclusions were hardly general. Other review papers appeared over time [4, 84]. Many aspects of heterogeneous catalysis can be treated, from deactivation and coke formation [85–87] to the identification of intermediate species [88, 89] and determination of the mechanism by reaction kinetics (combining the kinetics of surface processes with the usual time change analysis of the reaction products in the gas phase), sometimes with transient isotope labeling [90]. Kinetics have also been studied by imposing periodic variations

of reactant concentrations [91], creating a sort of imposed oscillatory reaction (which has also been studied on its own by *operando* IR spectroscopy [92]).

### 1.5.1

#### Experimental Setup for *Operando* IR Spectroscopy and Reactions Conditions

The reactor-cell must obey specific constraints for reactivity studies. The residence time must be controlled accurately, and the gas volume was chosen in some designs to be as small as possible in order to increase the time resolution of online analysis and to remove the contribution of the gas phase to the spectrum.

*Operando* IR spectroscopy is most often applied to gas–solid heterogeneous catalysis. The contribution of the gas phase to the IR spectrum can then be taken into account and removed from the spectrum of the surface of the solid. The typical setup is very similar to the usual setup for catalytic tests. It includes gas mixing devices (mass flow regulators with automatic control), the reactor (here with IR windows), and online gas analysis techniques (mass spectrometry, gas chromatography, chemoluminescence, IR gas analysis, etc.) (Figure 1.31).

The main difference between the *operando* IR setup and any usual catalysis test setup is the limit to the reaction conditions imposed by the use of IR windows. In order to maintain gas tightness between 1 and 10–20 atm, gaskets must be placed between the KBr or CaF<sub>2</sub> windows and the cell walls. Most gasket materials can only be used below 200 °C, and the design of the reactor cell must include a careful design of the heating so that the temperature is homogeneous enough around the catalyst, with cooling of the windows and gaskets (Figure 1.32). This must be combined with a small dead volume around the solid catalyst so that the kinetic behavior of the reactor can be analyzed with the best possible time resolution. With a short residence time for reactants inside the reactor, a fast spectroscopic measurement on the surface combined with fast online analysis techniques can lead to a detailed description of complex kinetics on the surface [93].

### 1.5.2

#### Examples of *Operando* IR Measurements

When studied under reaction conditions, the surface of metal oxides is often covered by unreactive species called “spectators,” which do not participate in the reaction of interest. This means that only a few of the surface sites are really catalytically active. This was observed, for instance, in the hydrogenation of methyl benzoate to benzaldehyde on various metal oxides: on ZrO<sub>2</sub> under working conditions, IR spectroscopy showed the presence of large amount of benzoate species, mostly inactive towards H<sub>2</sub>.

Zeolitic materials are very convenient for active site identification since the Brønsted sites are characterized by well-defined  $\nu(\text{OH})$  bands. On dealuminated HY samples (at 673 K under flow) it was shown that *n*-hexane cracking was related to OH groups characterized by a  $\nu(\text{OH})$  at 3600 cm<sup>-1</sup>, assigned to strongly acidic hydroxyl groups that correspond to framework OH groups perturbed by extra-

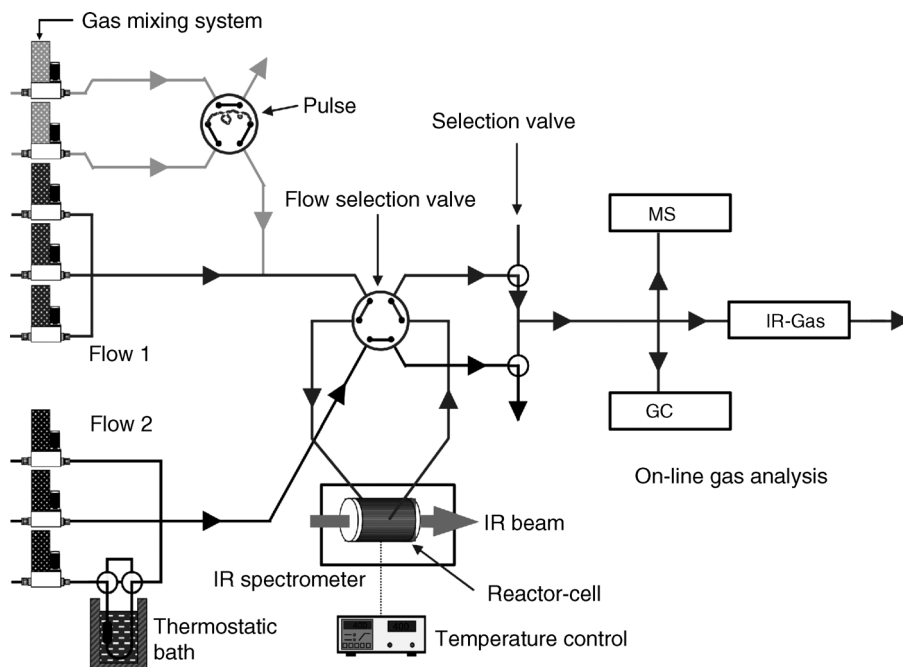


**Figure 1.31** Typical *operando* IR setup. Mass flow regulators are used to prepare gas mixtures that are sent in the reactor cell. Several separate flows are often used to allow fast switching between different gas mixtures for time-resolved studies of fast transients. Six-way valves are used for switching between flows or for sending 10–100  $\mu\text{l}$  pulses without disturbing the main flow in the reactor. A saturator is used

for introducing liquids in the flow (by passing the carrier gas in a loop where the liquid is placed, in a thermostatic bath – the flow is then loaded with the vapor pressure of the liquid at the temperature of the bath – the gas lines must then be heated slightly higher than the bath). The flows exiting the reactor are then directed via a selection valve to the chosen online gas analysis technique.

framework species. Moreover, poisoning experiments with DMP confirmed the involvement of these sites [94].

Alumina-based additives are used on an industrial scale to reduce the amount of sulfur in fluid catalytically cracked (FCC) gasoline. Recent *operando* IR studies allowed the elucidation of the mechanism by which gasoline sulfur-reductive additives reduce thiophenic compounds [95]. Recording the surface species during the reaction of tetrahydrothiophene decomposition and measuring the evolution of the conversion versus time-on-stream showed that the accumulation of carboxylate is at the origin of catalyst deactivation (Figure 1.33). The *operando* setup also allows control poisoning of the strongest Lewis acid that clearly shows their implication in catalytic activity. Hence tetrahydrothiophene (THT) cracking requires both Lewis acid and basic sites. The involvement of strong tetrahedral  $\text{Al}^{3+}$  sites has been directly evidenced by specific poisoning using pyridine under reaction conditions. A strong indication that basic sites are also involved in the reaction mechanism is the

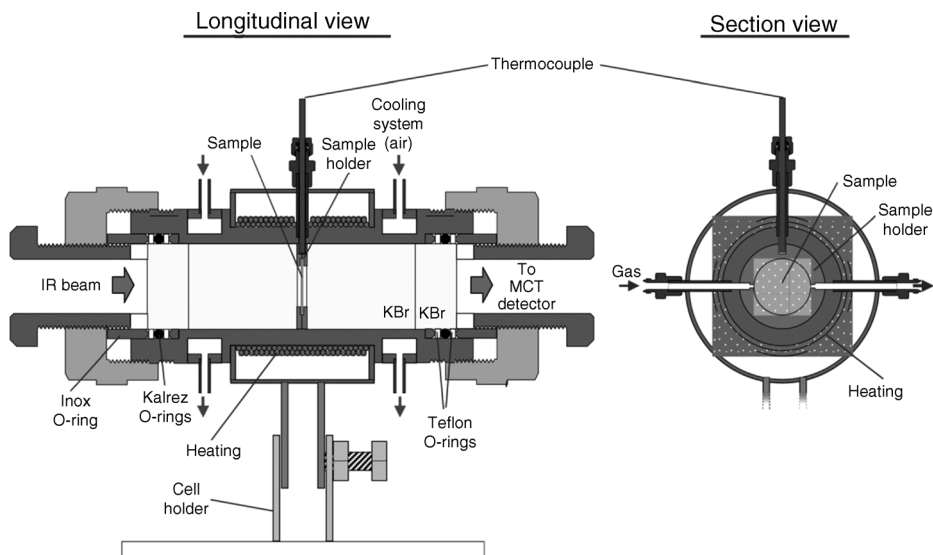


**Figure 1.32** Operando reactor cell for experiments in the range 25–450 °C, 1–20 atm, gas velocity up to 70 000 h<sup>-1</sup>. The dead volume is <0.1 ml. From [93].

fact that deactivation originates from the formation of carboxylate species, leading to blocking of surface oxygen centers. Overall, these results show that a good balance of the acid–base properties of alumina-based additive is required for optimum activity, suggesting that THT cracking occurs on Lewis acid–base pairs through successive *E2* eliminations.

The *operando* setup is well adapted to transient experiments. As a simple example, in a flow of propane and O<sub>2</sub> at 623 K on a VPO/TiO<sub>2</sub> catalyst, it was observed that introduction of a pulse of pyridine drastically decreased the activity. When the

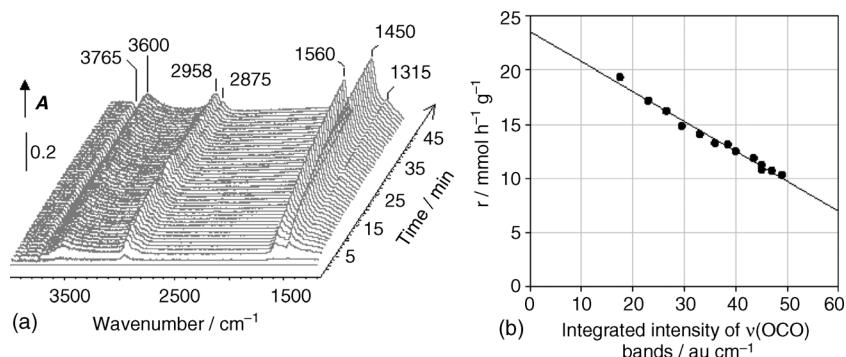


**Figure 1.33** (a) IR spectra recorded during THT conversion on alumina at 688 K. (b) THT conversion versus surface of the carboxylate  $\nu(\text{OCO})$  bands [the units for integrated intensity are absorbance unit (au) cm<sup>-1</sup>]. From [95].

pyridine flow was stopped, IR spectroscopy showed that Lewis acid sites were preferentially recovered, whereas the CO<sub>2</sub> selectively increased, indicating that CO<sub>2</sub> formation was linked to Lewis sites presence whereas Brønsted sites were linked to propene formation [96].

The state of the adsorbed reactant can sometimes directly be an indication of the state of the active sites under reaction conditions. In the CO conversion reaction on zeolite-supported Pt catalysts at various stages of aging, the reactant is at the same time the probe molecule [97]. When a temperature-programmed reaction is studied by *operando* IR spectroscopy [CO (4000 ppm)–O<sub>2</sub> (12 000 ppm) in 30 ml min<sup>-1</sup> Ar, gas velocity 60 000 h<sup>-1</sup>, 298–523 K], oxidized Pt (Pt<sup>δ+</sup>) is first detected on the aged catalyst, with the formation of dicarbonyls. The frequency of the ν(CO) vibration band is a clear indicator of the state of the Pt atoms (Figure 1.34). The complex feature for the CO bands was analyzed by chemometrics [multivariate curve resolution (MCR)]. Heating in the reactant flow induces the transformation of dicarbonyls into monocarbonyls, and further reduction of the Pt particles. The conversion is monitored at the same time, and the light off is observed when the temperature is high enough on the reduced Pt catalyst.

Very high time resolution (~10 ns) can be achieved by special recording techniques such as step scan interferometry. Step scan interferometry only records one point of the interferogram over time, and the measurement has to be repeated many times so that all the points in the interferogram can be collected. The IR spectra themselves are obtained after Fourier transformation of all the recomposed interferograms. The catalytic experiment therefore needs to be well controlled in time but also highly reproducible. If the start of the reaction is well controlled in time, the various states of the surface can be recorded over time and the observation can be reproduced so that results are co-added to lower the detection limit. Fast valves allow millisecond control over the reaction, which can be coupled with millisecond step

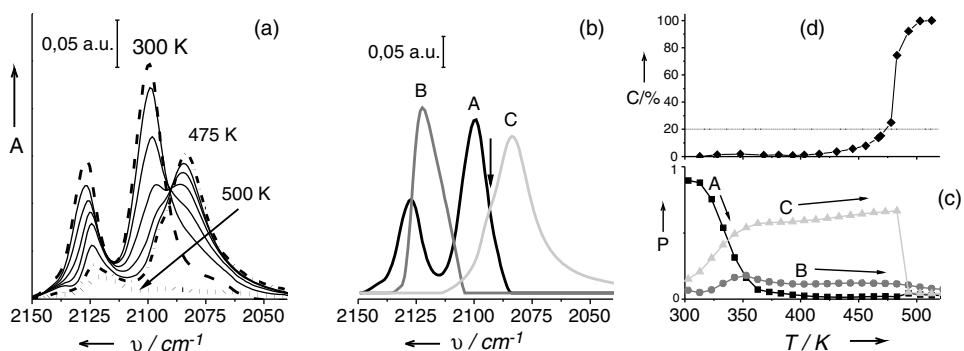


**Figure 1.34** (a) IR spectra obtained during the heating ramp after addition of CO–O<sub>2</sub> mixture on an aged catalyst, (b) corresponding MCR decomposition into three reference spectra, where A is the Pt<sup>δ+</sup> dicarbonyl, B is the Pt<sup>δ+</sup> monocarbonyl, and C is the CO on Pt<sup>0</sup>, and

(c) concentration profiles. *P* is dimensionless and expressed as the relative contribution of the three reference spectra in (b) to the spectra displayed in (a). (d) The conversion of CO into CO<sub>2</sub> (C %). From [97].

scan interferometry [98]. Nanosecond control of a reaction is achieved with laser-triggered reaction, mostly in photochemistry [99]. Thermal reactions can also be observed, and a laser can provide the heat necessary to induce a reaction followed by step scan FTIR spectroscopy at the nanosecond time scale. Measuring the conversion and selectivity is not really possible under such conditions, because online analysis techniques can hardly follow such a small “reaction pulse,” but these studies can be combined with slower but real *operando* measurements.

The importance of isocyanate species in the pathway from  $C_2H_5OH + NO + O_2$  reaction to  $N_2$  formation on an  $Ag/Al_2O_3$  sample was established with true *operando* measurements (temperature-programmed reaction from 623 to 923 K, NO 500 ppm, EtOH 1000 ppm,  $O_2$  10%; W/F =  $0.048 \text{ g s cm}^{-3}$ , conversion measured by online mass spectrometry) [100]. The coordination and transformation sites were determined via the use of isotopically labeled species in IR spectroscopy [101]. In a second study, the reaction of CO and NO on Ag supported on alumina was induced by an ultrafast pulsed laser, after which the state of the adsorbed species was monitored by step scan FTIR spectroscopy with 33 ns time resolution [102] (Figure 1.35). The reaction was studied in a closed reactor, with CO and NO at a partial pressure of 10 mbar. The system was at 473 K, and the laser provided the additional heat to induce the reaction. The transformation of cyanides on silver into isocyanates on alumina is the limiting step of the reaction. This step could be recorded, and a bridged intermediate was detected between the silver particle and the alumina surface. This intermediate only lasts 2  $\mu\text{s}$ , and it leads to the formation of an isocyanide on  $Al^{VI}$  ( $Al^{VI}$  is statistically the most accessible site), which in turn is quickly oxidized to an isocyanate and transferred to the stronger Lewis acid  $Al^{IV}$ . The interface between the

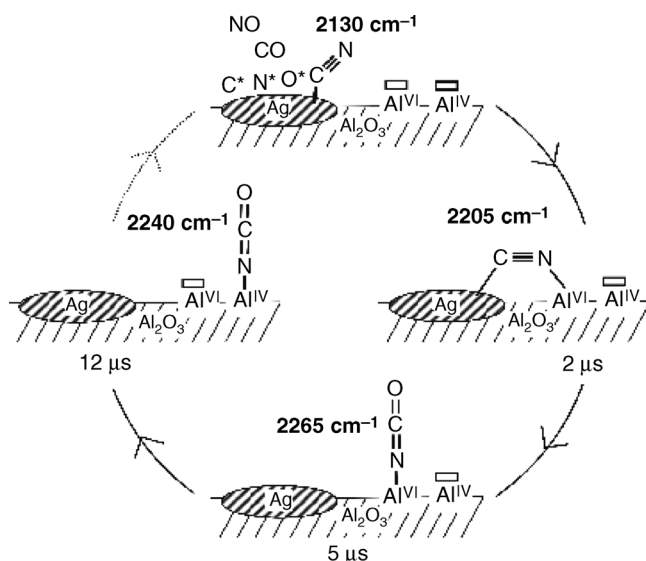


**Figure 1.35** Mechanism of the reaction of cyanide species on alumina-supported silver catalysts in a  $deNO_x$  reaction as seen by real time IR spectroscopy in the reactor. After [102]

Ag particle and the alumina support plays a key role in the catalytic activity, and this helps in understanding the role of the particle size.

Many other examples can be found in the literature, and a complete description of the procedure for IR characterization of the working catalyst has been extensively described in a recent review on the characterization of catalytically active sites by IR spectroscopy [5].

## 1.6

### Conclusion

IR spectroscopy is widely available in the laboratory. The spectrometer is not expensive, and measurements are easy. This has made IR spectroscopy one of the basic techniques for the characterization of solids, especially for heterogeneous catalysis. The surface properties of the solid can be measured by using a suitable probe molecule, and information can be obtained on the acid–base properties and on the metal sites. New developments have appeared with combined techniques (e.g., IR spectroscopy and gravimetry). IR spectroscopy has been used for more than 20 years to study surface reactivity. Catalytic reactors can be equipped with IR windows, to study the solid under reaction conditions. Elementary steps in heterogeneous catalysis can thus be observed, and IR spectroscopy is now established as one of the main tools in understanding heterogeneous catalysis. Optical and molecular spectroscopies such as infrared might still become more important with the coming of TeraHertz spectroscopy, bridging the gap towards the very far infrared and the microwaves and bringing a whole new domain for understanding heterogeneous catalysis.

### References

- 1 Herschel, W. (1800) *Philos. Trans. R. Soc. London*, **90**, 284–292.
- 2 Herschel, W. and Dreyer, J.L.E. (1912) *The Scientific Papers of Sir William Herschel*, Royal Society and Royal Astronomical Society, London.
- 3 Baddour, R.F., Modell, M., and Goldsmith, R.L. (1970) *J. Phys. Chem.*, **74**, 1787–1796.
- 4 Thibault-Starzyk, F. and Saussey, J. (2004) in *In Situ Characterization of Catalysts* (ed. B.M. Weckhuysen), American Scientific Publishers, Stevenson Ranch, CA, pp. 15–31.
- 5 Vimont, A., Thibault-Starzyk, F., and Daturi, M. (2010) *Chem. Soc. Rev.*, **39**, 4928–4950.
- 6 Morterra, C., Magnacca, G., and Bolis, V. (2001) *Catal. Today*, **70**, 43–58.
- 7 Flanigen, E.M. (1976) in *Zeolite Chemistry and Catalysis* (ed. J.A. Rabo), American Chemical Society, Washington, DC, pp. 80–117.
- 8 Sohn, J.R., Decanio, S.J., and Lunsford, J.H. (1986) *Zeolites*, **6**, 225–227.
- 9 Cairon, O., Khabtou, S., Balanzat, E., Janin, A., Marzin, M., Chambellan, A., Lavalley, J.C., and Chevreau, T. (1994) *Stud. Surf. Sci. Catal.*, **84**, 997–1004.
- 10 Maache, M., Janin, A., Lavalley, J.C., Joly, J.F., and Benazzi, E. (1993) *Zeolites*, **13**, 419–426.
- 11 Maache, M., Janin, A., Lavalley, J.C., and Benazzi, E. (1995) *Zeolites*, **15**, 507–516.
- 12 Thibault-Starzyk, F., Janin, A., and Lavalley, J.C. (1997) *Angew. Chem. Int. Ed. Engl.*, **36**, 989–991.

- 13 Crépeau, G., Montouillout, V., Vimont, A., Mariey, L., Cseri, T., and Maugé, F. (2006) *J. Phys. Chem. B*, **110**, 15172–15185.
- 14 Tsyganenko, A.A. and Filimonov, V.N. (1973) *J. Mol. Struct.*, **19**, 579–589.
- 15 Knözinger, H. and Ratnasamy, P. (1978) *Catal. Rev.*, **17**, 31–70.
- 16 Digne, M., Sautet, P., Raybaud, P., Euzen, P., and Toulhoat, H. (2002) *J. Catal.*, **211**, 1–5.
- 17 Knoezinger, H. (1993) in *Elementary Reaction Steps in Heterogeneous Catalysis* (eds R.W. Joyner and R.A. Van Santen), Kluwer, Dordrecht, pp. 267–285.
- 18 Lercher, J.A., Grundling, C., and Edermirth, G. (1996) *Catal. Today*, **27**, 353–376.
- 19 Knozinger, H. and Huber, S. (1998) *J. Chem. Soc. Faraday Trans.*, **94**, 2047–2059.
- 20 Donoso-Tauda, O., Jaque, P., and Santos, J.C. (2011) *Phys. Chem. Chem. Phys.*, **13**, 1552–1559.
- 21 Lavalley, J.C., Jolly-Feaugas, S., Janin, A., and Saussey, J. (1997) *Mikrochim. Acta (Suppl.)*, **14**, 51–56.
- 22 Rouxhet, P.G. and Sempels, R.E. (1974) *J. Chem. Soc. Faraday Trans.*, **70**, 2021–2032.
- 23 Evans, J.C. and Wright, N. (1960) *Spectrochim. Acta, Part A*, **16**, 352–357.
- 24 Bratos, S. and Ratajczak, H. (1982) *J. Chem. Phys.*, **76**, 77–85.
- 25 Pelmeshnikov, A.G., van Wolput, J.H.M.C., Janchen, J., and van Santen, R.A. (1995) *J. Phys. Chem.*, **99**, 3612–3617.
- 26 Claydon, M.F. and Sheppard, N. (1969) *J. Chem. Soc., Chem. Commun.*, 1431–1433.
- 27 Maugé, F., Sahibed-Dine, A., Gaillard, M., and Ziolek, M. (2002) *J. Catal.*, **207**, 353–360.
- 28 Travert, A., Manoilova, O.V., Tsyganenko, A.A., Maugé, F., and Lavalley, J.C. (2002) *J. Phys. Chem. B*, **106**, 1350–1362.
- 29 Vimont, A., Leclerc, H., Maugé, F., Daturi, M., Lavalley, J.-C., Surblé, S., Serre, C., and Férey, G. (2007) *J. Phys. Chem. C*, **111**, 383–388.
- 30 Thibault-Starzyk, F., Payen, R., and Lavalley, J.C. (1996) *Chem. Commun.*, 2667–2668.
- 31 Thibault-Starzyk, F., Bettahar, M.M., Saussey, J., and Lavalley, J.C. (1997) *Stud. Surf. Sci. Catal.*, **105**, 925–931.
- 32 Glazunov, V.P. and Odinkov, S.E. (1982) *Spectrochim. Acta*, **38**, 399–408.
- 33 Odinkov, S.E., Mashkovsky, A.A., Glazunov, V.P., Iogansen, A.V., and Rassadin, B.V. (1976) *Spectrochim. Acta*, **32**, 1355–1363.
- 34 Janin, A., Maache, M., Lavalley, J.C., Joly, J.F., Raatz, F., and Szydowski, N. (1991) *Zeolites*, **11**, 391–396.
- 35 Khabtou, S., Chevreau, T., and Lavalley, J.C. (1994) *Micropor. Mesopor. Mater.*, **3**, 133–148.
- 36 Travert, A., Vimont, A., Sahibed-Dine, A., Daturi, M., and Lavalley, J.-C. (2006) *Appl. Catal. A: Gen.*, **307**, 98–107.
- 37 Hunter, E.P.L. and Lias, S.G. (1998) *J. Phys. Chem. Ref. Data*, **27**, 413–657.
- 38 Jacobs, P.A. and Heylen, C.F. (1974) *J. Catal.*, **34**, 267–274.
- 39 Morterra, C., Cerrato, G., and Meligrana, G. (2001) *Langmuir*, **17**, 7053–7060.
- 40 Lahousse, C., Aboulayt, A., Maugé, F., Bachelier, J., and Lavalley, J.C. (1993) *J. Mol. Catal.*, **84**, 283–297.
- 41 Oliviero, L., Vimont, A., Lavalley, J.-C., Romero Sarria, F., Gaillard, M., and Mauge, F. (2005) *Phys. Chem. Chem. Phys.*, **7**, 1861–1869.
- 42 Onfroy, T., Clet, G., Bukallah, S.B., Visser, T., and Houalla, M. (2006) *Appl. Catal. A: Gen.*, **298**, 80–87.
- 43 Thibault-Starzyk, F., Stan, I., Abelló, S., Bonilla, A., Thomas, K., Fernandez, C., Gilson, J.-P., and Pérez-Ramírez, J. (2009) *J. Catal.*, **264**, 11–14.
- 44 Daniell, W., Topsoe, N.Y., and Knozinger, H. (2001) *Langmuir*, **17**, 6233–6239.
- 45 Bolis, V., Fubini, B., Garrone, E., and Morterra, C. (1989) *J. Chem. Soc. Faraday Trans. 1*, **85**, 1383–1395.
- 46 Hadjiivanov, K.I. and Vayssilov, G.N. (2002) *Adv. Catal.*, **47**, 307–511.
- 47 Cairon, O. and Chevreau, T. (1998) *J. Chem. Soc. Faraday Trans.*, **94**, 323–330.
- 48 Chevreau, T., Cairon, O., Janin, A., and Lavalley, J.C. (1996) *J. Chim. Phys. Phys. Chim. Biol.*, **93**, 355–372.

- 49 Marie, O., Massiani, P., and Thibault-Starzyk, F. (2004) *J. Phys. Chem. B*, **108**, 5073–5081.
- 50 Nesterenko, N.S., Thibault-Starzyk, F., Montouillout, V., Yushchenko, V.V., Fernandez, C., Gilson, J.-P., Fajula, F., and Ivanova, I.I. (2004) *Micropor. Mesopor. Mater.*, **71**, 157–166.
- 51 Nesterenko, N.S., Thibault-Starzyk, F., Montouillout, V., Yushchenko, V.V., Fernandez, C., Gilson, J.-P., Fajula, F., and Ivanova, I.I. (2006) *Kinet. Catal.*, **47**, 40–48.
- 52 Soltanov, R.I., Paukshtis, E.A., and Yurchenko, E.N. (1987) *React. Kinet. Catal. Lett.*, **34**, 421–426.
- 53 Pelmentschikov, A.G., van Santen, R.A., Jänchen, J., and Meijer, E.L. (1993) *J. Phys. Chem.*, **97**, 11071–11074.
- 54 Jolly, S., Saussey, J., and Lavalley, J.C. (1994) *Catal. Lett.*, **24**, 141–146.
- 55 Anquetil, R., Saussey, J., and Lavalley, J.C. (1999) *Phys. Chem. Chem. Phys.*, **1**, 555–560.
- 56 Thibault-Starzyk, F., Travert, A., Saussey, J., and Lavalley, J.C. (1998) *Top. Catal.*, **6**, 111–118.
- 57 Zecchina, A., Marchese, L., Bordiga, S., Paze, C., and Gianotti, E. (1997) *J. Phys. Chem. B*, **101**, 10128–10135.
- 58 Lavalley, J.C. (1996) *Catal. Today*, **27**, 377–401.
- 59 Barthomeuf, D. (1996) *Catal. Rev. Sci. Eng.*, **38**, 521–612.
- 60 Vimont, A., Thibault-Starzyk, F., and Lavalley, J.C. (2000) *J. Phys. Chem. B*, **104**, 286–291.
- 61 Bachelier, J., Aboulayt, A., Lavalley, J.C., Legendre, O., and Luck, F. (1993) *Catal. Today*, **17**, 55–62.
- 62 Bensitel, M., Saur, O., and Lavalley, J.C. (1991) *Mater. Chem. Phys.*, **28**, 309–320.
- 63 Daturi, M., Binet, C., Lavalley, J.C., and Blanchard, G. (2000) *Surf. Interface Anal.*, **30**, 273–277.
- 64 Sánchez-Sánchez, M. and Blasco, T. (2009) *Catal. Today*, **143**, 293–301.
- 65 Kuhn, J.N. and Ozkan, U.S. (2008) *J. Catal.*, **253**, 200–211.
- 66 Moulin, B., Oliviero, L., Bazin, P., Daturi, M., Costentin, G., and Maugé, F. (2010) *Phys. Chem.*, **13**, 10797–10807.
- 67 Petitjean, H., Tarasov, K., Delbecq, F., Sautet, P., Krafft, J.M., Bazin, P., Paganini, M.C., Giamello, E., Che, M., Lauron-Pernot, H., and Costentin, G. (2010) *J. Phys. Chem. C*, **114**, 3008–3016.
- 68 Chizallet, C., Costentin, G., Che, M., Delbecq, F., and Sautet, P. (2006) *J. Phys. Chem. B*, **110**, 15878–15886.
- 69 Branda, M.M., Ferullo, R.M., Belelli, P.G., and Castellani, N.J. (2003) *Surf. Sci.*, **527**, 89–99.
- 70 Hadjiivanov, K. (2000) *Catal. Rev. Sci. Eng.*, **42**, 71–144.
- 71 Maugé, F., Binet, C., and Lavalley, J.C. (1997) in *Catalysis by Metals*, (eds A.-J. Renouprez and H. Jobic), Les Éditions de Physique, Paris, pp. 3–27.
- 72 Hollins, F. P. (1992) *Surf. Sci. Rep.*, **16**, 51–94.
- 73 Yates, J.T. Jr (1994) *Surf. Sci.*, **299–300**, 731–741.
- 74 Binet, C., Jadi, A., and Lavalley, J.-C. (1989) *J. Chim. Phys. Phys. Chim. Biol.*, **86**, 451–470.
- 75 Oliviero, L., Mariey, L., Lélias, M.A., Aiello, S., Gestel, J., and Maugé, F. (2010) *Catal. Lett.*, **135**, 62–67.
- 76 Koizumi, N., Yamazaki, M., Hatanaka, S., and Yamada, M. (1997) *Catal. Today*, **39**, 33–44.
- 77 Topsøe, H., Clausen, B.S., and Massoth, F.E. (1996) *Hydrotreating Catalysis*, Springer, Berlin.
- 78 Travert, A., Dujardin, C., Maugé, F., Veilly, E., Cristol, S., Paul, J.-F., and Payen, E. (2006) *J. Phys. Chem.*, **110**, 1261–1270.
- 79 Dujardin, C., Lelias, M.A., van Gestel, J., Travert, A., Duchet, J.C., and Maugé, F. (2007) *Appl. Catal.*, **322**, 46–57.
- 80 Lelias, M.A., Kooyman, P.J., Mariey, L., Oliviero, L., Travert, A., van Gestel, J., van Veen, J.A.R., and Mauge, F. (2009) *J. Catal.*, **267**, 14–23.
- 81 Thibault-Starzyk, F., Gil, B., Aiello, S., Chevreau, T., and Gilson, J.-P. (2004) *Micropor. Mesopor. Mater.*, **67**, 107–112.
- 82 Gallas, J.-P., Goupil, J.-M., Vimont, A., Lavalley, J.-C., Gil, B., Gilson, J.-P., and Miserque, O. (2009) *Langmuir*, **25**, 5825–5834.
- 83 Bazin, P., Alenda, A., and Thibault-Starzyk, F. (2010) *Dalton Trans.*, **39**, 8432–8436.

- 84 Weckhuysen, B.M. (2002) *Chem. Commun.*, 97–110.
- 85 Karge, H.G., Niessen, W., and Bludau, H. (1996) *Appl. Catal. A: Gen.*, **146**, 339–349.
- 86 Vimont, A., Thibault-Starzyk, F., and Lavalley, J.C. (2000) *Stud. Surf. Sci. Catal.*, **130**, 2963–2969.
- 87 Vimont, A., Marie, O., Gilson, J.P., Saussey, J., Thibault-Starzyk, F., and Lavalley, J.C. (1999) *Stud. Surf. Sci. Catal.*, **126**, 147–154.
- 88 Centi, G., Perathoner, S., and Tonini, S. (2000) *Catal. Today*, **61**, 211–221.
- 89 Amblard, M., Burch, R., and Southward, B.W.L. (2000) *Catal. Today*, **59**, 365–371.
- 90 Meunier, F.C., Tibiletti, D., Goguet, A., Shekhtman, S., Hardacre, C., and Burch, R. (2007) *Catal. Today*, **126**, 143–147.
- 91 Ortelli, E.E., Wambach, J., and Wokaun, A. (2000) *Appl. Catal. A: Gen.*, **192**, 137–152.
- 92 Miners, J.H., Martin, R., Gardner, P., Nalezinski, R., and Bradshaw, A.M. (1997) *Surf. Sci.*, **377**, 791–795.
- 93 Lesage, T., Verrier, C., Bazin, P., Saussey, J., and Daturi, M. (2003) *Phys. Chem. Chem. Phys.*, **5**, 4435–4440.
- 94 Jolly, S., Saussey, J., and Lavalley, J.C. (1994) *J. Mol. Catal.*, **86**, 401–421.
- 95 Can, F., Travert, A., Ruau, V., Gilson, J.-P., Maugé, F., Hu, R., and Wormsbecher, R.F. (2007) *J. Catal.*, **249**, 79–92.
- 96 Savary, L., Saussey, J., Costentin, G., Bettahar, M., and Gubelmann Bonneau, M. (1996) *Catal. Today*, **32**, 57–61.
- 97 Rivallan, M., Thomas, S., Lepage, M., Takagi, N., Hirata, H., and Thibault-Starzyk, F. (2010) *ChemCatChem*, **2**, 1599–1605.
- 98 Wasylenko, W. and Frei, H. (2007) *Phys. Chem. Chem. Phys.*, **9**, 5497–5502.
- 99 Frei, H. and Yeom, Y.H. (2004) in *In Situ Spectroscopy of Catalysts* (ed. B. Weckhuysen), American Scientific Publishers, Stevenson Ranch, CA, pp. 20–34.
- 100 Bion, F N, Saussey, J., Haneda, M., and Daturi, M. (2003) *J. Catal.*, **217**, 47–58.
- 101 Bion, N., Saussey, J., Hedouin, C., Seguelong, T., and Daturi, M. (2001) *Phys. Chem. Chem. Phys.*, **3**, 4811–4816.
- 102 Thibault-Starzyk, F., Seguin, E., Thomas, S., Daturi, M., Arnolds, H., and King, D.A. (2009) *Science*, **324**, 1048–1051.